IEEE Access
Multidisciplinary | Rapid Review | Open Access Journal

Received 16 December 2024, accepted 25 December 2024, date of publication 10 January 2025, date of current version 23 January 2025.

Digital Object Identifier 10.1109/ACCESS.2025.3528343

RESEARCH ARTICLE

Matching Sensing to Actuation and Dynamics in Distributed Sensorimotor Architectures

ZOE TURIN[1], GRAHAM K. TAYLOR[2], HOLGER G. KRAPP[3], EMILY JENSEN[4], (Member, IEEE), AND J. SEAN HUMBERT[1], (Member, IEEE)

[1]Department of Mechanical Engineering, University of Colorado Boulder (UCB), Boulder, CO 80303, USA
[2]Department of Biology, University of Oxford, OX1 3SZ Oxford, U.K.
[3]Department of Bioengineering, Imperial College London, South Kensington Campus, SW7 2AZ London, U.K.
[4]Department of Electrical, Computer and Energy Engineering, University of Colorado Boulder (UCB), Boulder, CO 80303, USA

Corresponding author: Zoe Turin (zoe.turin@colorado.edu)

This work was supported in part by the U.S. National Aeronautics and Space Administration under Grant 80NSSC19K1137, in part by the U.S. Air Force Research Laboratory (AFRL), in part by the Air Force Office of Scientific Research (AFOSR) under Grant FA-9550-14-1-0068, and in part by the European Office of Aerospace Research and Development (EOARD) through AFOSR under Grant FA-9550-09-1-0075.

ABSTRACT In this article we explore the benefits of matching sensing characteristics to actuation and dynamics in the context of spatially distributed sensorimotor architectures, motivated by recently discovered connections in blowfly flight physics and visual physiology. Within the proposed framework, we present novel semidefinite programs with linear matrix inequality constraints which yield directions encoded in the sensory output that maximize the smallest unstable Hankel singular value of the system. This is a coordinate-invariant metric that minimizes the control energy required to stabilize an unstable system and maximizes the achievable robustness to unstructured additive uncertainty over all possible controllers. We also reformulate the problem to achieve a prescribed speed of response, which can be applied to stable and unstable systems. We adapt a maximally robust controller synthesis method from previous work which provides a tool for validation. We additionally present an H_∞ controller formulation which allows for a trade-off between minimization of actuator effort and robustness versus disturbance rejection and tracking capability, providing design flexibility over the maximally robust controller.

INDEX TERMS Bio-inspired robotics, H infinity control, matched filters, semidefinite programming, sensor arrays, robust control.

I. INTRODUCTION

Natural systems have evolved to make effective reductions of rich and high-dimensional sensory data, forming simple representations that allow organisms to perform well with limited computational overheads in the presence of uncertainty. A ubiquitous underlying principle, which is better studied in less complex animals, is sensorimotor convergence [1], [2], [3]. In this architecture, spatio-temporal integration/correlation of local sensor signals both within and across sensory modalities enables extraction of time-varying signals that can be applied as feedback. In flies, individually identified neurons called Lobula Plate Tangential Cells (LPTCs) respond to optic flow fields matched to specific self-motions [4], [5], forming the output layer of what is presently nature's best-understood deep convolutional neural network [6], [7], [8]. The lateral line system in fish and other aquatics is another representative example, in which local fluid velocity or pressure difference measurements are pooled to extract motion and structure of the environment [9], [10]. In addition, insect wings generate complex spatiotemporal patterns of strain that are transduced by distributed mechanoreceptor arrays, the campaniform sensilla, whose placement determines the sensory information available to the animal [11], [12].

The sensorimotor convergence architecture described above has several important advantages, especially for systems that require fast sensory feedback to achieve

The associate editor coordinating the review of this manuscript and approving it for publication was Mouquan Shen.

robust behavior. Reduced estimate covariance is achieved through the instantaneous spatial weighting of individual measurements from the sensor array [13], [14], [15]. This in turn provides a reduction in latency and computational complexity, as signal-to-noise improvements through temporal averaging provided by a dynamic filter are not essential. The reduced complexity allows for implementations with potentially orders of magnitude improvement in size, weight, and power [16]. Additionally, outputs can be selected to encode dynamically significant directions in state space. Recent work in the modeling and analysis of the blowfly visuomotor system has shown that the LPTC pooling neurons are tuned to non-orthogonal, dynamically relevant directions of the animal, such as worst-case disturbance combinations or the most energetically efficient directions of motion in state space [17].

The last point hints at a principle that has rarely been explored or exploited in platform design: the tuning of sensing characteristics to match those of the actuation and dynamics of the system. Flight vehicle design methodology typically integrates sensing and feedback control at a late stage of the process, which can lead to sub-optimal maneuverability, efficiency, and closed-loop behavior. To improve performance, novel design tools and methodologies are required that allow the integration and optimization of sensing, actuation, and platform dynamics at the earliest stage of concept selection.

A. CONTRIBUTIONS

In this paper, we present a new approach to designing distributed sensing systems which adapts sensorimotor convergence architectures to engineered systems, and applies optimization objectives motivated by recently discovered connections between blowfly flight physics and visual physiology. This approach tunes the outputs of distributed sensing systems to the system dynamics and actuation.

Our contributions are as follows. First, we present a new semidefinite programming approach to optimize the directions encoded by a sensing system using novel objectives linked to closed-loop robustness and actuator authority. Second, we present a novel framework for distributed sensing synthesis that allows the information extracted to be tuned via spatial weighting patterns applied to the sensor measurements. Third, we adapt the optimization from our first contribution to synthesize spatial weighting patterns for generalized distributed sensing systems. Finally, we pair these contributions with existing control synthesis methods to realize improvements in closed-loop performance, which we demonstrate with several example systems. These contributions are discussed in the context of related work in Section II.

B. ORGANIZATION

The paper is organized as follows: related work is discussed in Section II, and Section III presents the mathematical notation used in this work. In Section IV, we review the required system-theoretic concepts and background. In Section V, we present a novel semidefinite programming approach to optimize the directions encoded by the sensing system. This formulation is extended to general distributed sensing systems in Section VI. In Section VII, we present a procedure for control synthesis which leverages the optimized open-loop tuning. In Section VIII, we conclude by applying the optimizations in Sections V and VI and the controller synthesis approaches in Section VII to some example flight systems that highlight the benefits of the proposed approach.

II. RELATED AND CURRENT WORK

The problem of co-tuning sensors, actuation, and dynamics is closely related to the problems of sensor and actuator placement and selection [18], which find extensive application in the areas of process control [19], power systems [20], flexible structures [21], networks [22], flow control [23], and resource planning [24].

Existing work in sensor placement and selection is largely aimed at minimizing an error metric for the state estimate or maximizing a metric of the observability of the system [25]. Examples include metrics based on maximum-likelihood state estimates [26] or eigenvalues of the observability Gramians [27]. A given objective may be to maximize the observability of the least observable mode [28] or the most observable mode [29], or be a balance of these two goals [30], [31]. Observability Gramian-based approaches have been examined for stable systems [27], [28], [30] and extended to unstable systems [29], [32] using the formulation for generalized Gramians given by [33]. Extensions to nonlinear systems through observability functions [28], observability covariances [27], unobservability indices [34], empirical observability Gramians [35] or stochastic observability Gramians [36] have also been considered.

Controllability and observability Gramians have been explored in conjunction but optimized independently for problems of sensor and actuator placement for an open-loop system, where sensor selection is based on maximizing signal energy in system outputs and actuator selection is based on minimizing input energy required to reach a given state [28], [29], [30], [32]. Measures based on geometric or subspace characteristics of the controllability and observability Gramians or resolvent analysis have also been employed [37], [38], [39].

As it is not obvious how to combine distinct measures of controllability and observability, additional metrics have been proposed that are functions of a system's Hankel singular values (HSVs), which quantify the amount of energy stored by a system through actuation and retrieved through sensing. These approaches attempt to optimize open-loop input-to-output behavior by (i) using HSVs to rank candidate sets of sensor/actuator pairings or placements [19], [20], [22], [40], [41], or (ii) balanced model reduction to rank sensor and actuator selections based on their joint controllability and observability [42].

Some of the existing work on HSV-based joint controllability and observability optimization has been limited to subclasses of systems. For example, related work applied to flexible structures uses standard assumptions about the underlying dynamics, including complex poles with small real parts (low damping) and non-clustered poles [43]. These assumptions allow for closed-form expressions of the HSVs [30], [44], [45], [46]. This is closely related and applied similarly to the open-loop H_2 and H_∞ norms of a structure [21], [47], [48] for sensor and actuator selection.

The methods described above reflect the perspective of optimizing properties the open-loop system, which then allows the designer to select the control structure and performance objectives independently. Alternative formulations that incorporate closed-loop performance as part of the optimization criteria in order to solve sensor and actuator selection and placement problems have also been considered.

The most widely used closed-loop objective is the H_2 norm which represents the output variance due to a white noise input. This has been applied to quantify disturbance rejection capability in sensor and actuator selection problems for static [49], [50] as well as dynamic [23], [51], [52], [53] feedback architectures. Linear quadratic Gaussian (LQG) control objectives, a special case of the H_2 control, have also been considered in [54] and [55]. The H_∞ norm, which measures the worst case energy gain for the closed-loop system, has been used as the basis for actuator selection for static [56] and dynamic [57] closed-loop architectures and for mixed H_2/H_∞ sensor and actuator design objectives in [58]. Lastly, sensor and actuator selection for closed-loop stability was examined in [59].

The aforementioned body of work largely concerns the optimal placement or selection of sensors and actuators, which due to its combinatorial nature requires evaluation of large numbers of candidate solutions. Furthermore, the problem is non-convex due to the boolean nature of sensor placement: a given sensor is either selected or not selected. Various solution methods have been proposed, including brute-force searches [60], branch-and-bound methods [55], [57], [58], convex relaxations [35], [61], genetic algorithms [32], [45], [52], and greedy selection techniques [22], [42], which may produce suboptimal results and may become impractical for large numbers of sensors.

The majority of the approaches outlined above also rely on controllabilty and/or observability measures as the objective functions. Notably, these quantities depend on the coordinates used to represent the state of the system. Typically, the system state is chosen for engineering convenience, but is not inherent to the system, e.g. body axes versus stability axes for the state of a flight system. Minimizing a metric of observability or controllability in one set of coordinates is not generally equivalent for the same system represented in different coordinates. Additionally, these metrics do not necessarily coincide with other important measures, e.g., closed-loop performance and robustness.

Related to the optimal placement/selection of sensors and actuators problems described above, we aim to solve a somewhat distinct problem: given a linear time-invariant (LTI) system with spatially distributed sensors, how do we select sensor weighting functions (sensitivity patterns) to match sensory characteristics to the actuation and dynamics of the open-loop system? Our inspiration is derived from the sensorimotor architectures of natural systems, in particular neurons that pool measurements across spatial arrays. In this case, the selection problem is considered over a continuous-valued set of spatial weightings that are applied to each sensor within an array, as opposed to a discrete (boolean) selection criterion as in the sensor selection problem.

The recently discovered relationship between blowfly flight physics and visual physiology provides additional insight as we show in Section V that the smallest unstable Hankel singular value is maximized in the animal's visuomotor system. This objective, maximizing the minimum unstable HSV, is a measure of joint observability and controllability and has been referenced as a potential objective for actuator and sensor selection [46], but to the authors' knowledge has not been explored as an objective function in existing literature.

In the seminal work of [62] and [63], the minimum unstable Hankel singular value is shown to be directly related to the amount of control energy required to stabilize an unstable system, and provides a lower bound on the H_∞ norm of the input demand closed-loop transfer function, $\|KS_o\|_\infty$. As such, it provides a coordinate-independent objective and a direct connection between open-loop characteristics and achievable closed-loop performance, without the need to explicitly synthesize a controller and evaluate the closed-loop objective function. By using this objective to optimize sensitivity patterns for distributed sensing systems, this work aims to both solve an outstanding problem in the design and processing of distributed sensing systems, and explore the optimization of a new metric of joint controllability-observability tied to closed-loop performance.

III. MATHEMATICAL NOTATION

Variables, Signals, Matrices

- (A, B, C): State space system with system matrix A, input matrix B, and output matrix C, with feedthrough matrix $D = 0$
- (A_s, B_s, C_s): Stable partition of the state space system (A, B, C) (9)
- (A_u, B_u, C_u): Unstable partition of the state space system (A, B, C) (9)
- K: Controller transfer function
- m: Number of outputs in a state space system
- n: Number of states in a state space system
- n_s: Number of stable modes in a state space system
- n_u: Number of unstable modes in a state space system (9)
- S_o: Output sensitivity transfer function

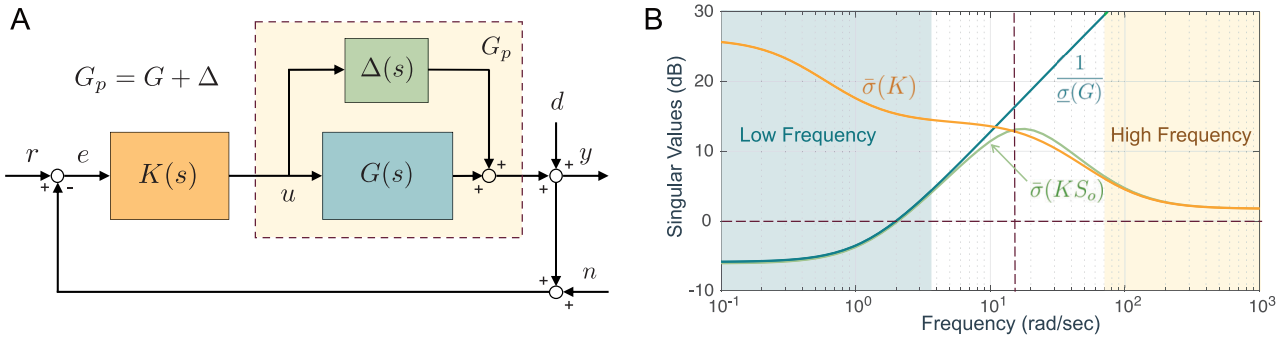

FIGURE 1. (A) Closed-loop Multi-Input Multi-Output (MIMO) feedback architecture with additive uncertainty. Signals r, n and d represent exogenous inputs while u, y, and e are internal signals. (B) Frequency response of the input demand transfer function KS_o with low and high frequency constraints.

- S_s, S_u: Stable and unstable partitions (17) of the inverse of the state space coordinate transformation which partitions the system into stable and unstable parts (9)
- T: State space coordinate transformation
- T_s, T_u: Stable and unstable partitions (16) of the state space coordinate transformation which partitions the system into stable and unstable parts (9)
- u: Input vector
- x: State vector
- $\bar{x}$: Equilibrium state
- X_c: Controllability Gramian (4) or generalized controllability Gramian [33]
- y: System output vector
- Y_o: Observability Gramian (5) or generalized observability Gramian [33]
- $\cdot^\star$: Optimum value of a variable, given an optimization problem

Elements of the Mathematical Framework for Distributed Sensing

- $\mathcal{B}$: Basis for function space $\mathcal{F}$
- $[\cdot]_\mathcal{B}, \cdot_\mathcal{B}$: Representation in basis $\mathcal{B}$ (30)
- $\mathcal{F}$: Function space of the measurement field and sensitivity patterns (21)
- g: Measurement field
- J: Measurement field Jacobian (29)
- q: Dimension of measurement field g
- γ: Generalized spatial coordinate
- Γ: Domain of generalized spatial coordinate γ
- ϕ_i: ith sensitivity pattern
- Φ: Matrix representation of a set of sensitivity patterns $\{\phi_i\}$

Standard Spaces

- $\mathcal{P}^n$: Space of positive semidefinite matrices of dimension $n \times n$

Functions and Operators

- $h_i(\cdot)$: i^{th} Hankel singular value of a state space system
- $\underline{h}(\cdot)$: Minimum Hankel singular value of a state space system
- $\mathcal{N}(\cdot)$: Null space
- $\mathcal{R}(\cdot)$: Range
- $X_c(\cdot)$: Controllability Gramian (4) or generalized controllability Gramian [33] of a state space system
- $Y_o(\cdot)$: Observability Gramian (5) or generalized observability Gramian [33] of a state space system
- $\lambda_i(\cdot)$: i^{th} eigenvalue of a matrix
- $\cap(\cdot\,,\,\cdot)$: Operator which returns a projection onto the intersection of the rowspaces of the projection matrices provided as arguments (40)
- $\langle\cdot\,,\,\cdot\rangle$: Inner product
- $(\cdot)^\dagger$: Moore-Penrose pseudoinverse
- $(\cdot)^*$: The reflection of a transfer function, e.g. $G = (A, B, C)$, $G^* = (-A, B, C)$

IV. SYSTEM-THEORETIC PRELIMINARIES

In this section, we introduce several system-theoretic concepts and notation common to the remainder of the paper. For a dynamical system, a linear time-invariant (LTI) state space model which describes the time evolution of the system state $x \in \mathbb{R}^n$ and its output $y \in \mathbb{R}^m$ is given by

$$\dot{x} = Ax + Bu \tag{1}$$

$$y = Cx + Du. \tag{2}$$

Collectively the state equation (1) and output equation (2) describe the transfer of signal energy from control inputs to sensor outputs. Here, $A \in \mathbb{R}^{n\times n}$ is the dynamics matrix, which characterizes the system response to perturbations in its state x, $B \in \mathbb{R}^{n\times p}$ is the control matrix which characterizes the response to inputs $u \in \mathbb{R}^p$, $C \in \mathbb{R}^{m\times n}$ is the output matrix which characterizes how the system state x is encoded by sensor outputs y, and $D \in \mathbb{R}^{m\times p}$ is the feedthrough matrix mapping inputs u to outputs y. In the following, we assume that the outputs are purely a function of the state x and not the input u, hence $D = 0$. The notation $G(s) = (A, B, C)$ refers to the system in the frequency domain,

$$G(s) = C(sI - A)^{-1}B = \left(\begin{array}{c|c} A & B \\ \hline C & 0 \end{array}\right). \tag{3}$$

A. DYNAMICALLY SIGNIFICANT DIRECTIONS IN STATE SPACE

The Gramians constructed from the A, B, and C system matrices encode the signal energy flow properties of a

system. When the system matrix A is stable, the real, symmetric controllability X_c and observability Y_o Gramians are defined as:

$$X_c = \int_0^\infty e^{A\tau} B B^T e^{A^T\tau} d\tau \tag{4}$$

$$Y_o = \int_0^\infty e^{A^T\tau} C^T C e^{A\tau} d\tau. \tag{5}$$

The Gramians are generated by computing the solutions to the Lyanunov equations,

$$AX_c + X_c A^T + BB^T = 0 \tag{6}$$

$$A^T Y_o + Y_o A + C^T C = 0. \tag{7}$$

The controllability Gramian has a direct connection with the minimum energy required to reach a given state x_0, which can be expressed as $\|u_{\text{opt}}\|_2^2 = x_0^T X_c^{-1} x_0$. By extension, the controllability ellipsoid $\mathcal{E}_c = \{x \in \mathbb{R}^n;\ x^T X_c^{-1} x \leq 1\}$ contains the region of state space that can be reached by applying inputs with unit norm $\|u\|_2 \leq 1$ [64]. The directions and lengths of the principal axes of $\mathcal{E}_c$ are determined by the eigenvectors and square roots of the eigenvalues of X_c. Hence, its longest axes represent the directions in state space requiring the least control effort to move along.

The observability Gramian has a direct connection to the output energy for a given initial condition x_0, as the energy of the output signal $y(t)$ for an arbitrary x_0 can be expressed as $\|y\|^2 = x_0^T Y_o x_0$. The set of initial conditions where $\|y\|_2^2 \leq 1$ yields the directions in state space that have the smallest output norm. If we replace Y_o with its inverse, then we can form the observability ellipsoid $\mathcal{E}_o = \{x \in \mathbb{R}^n; x^T Y_o^{-1} x \leq 1\}$. The principal axes of $\mathcal{E}_o$ represent the directions in state space that yield the largest output norm, characterizing the specific self-motions that the system is best able to sense. Additionally, $Y_o^{-1} = E\{[x(t) - \hat{x}(t)][x(t) - \hat{x}(t)]^T\}$ is the covariance of the best unbiased estimate $\hat{x}(t)$ based on the measurement $\{y(t),\ 0 < t < \infty\}$ that minimizes the scalar cost function $J = \text{trace}(Y_o^{-1}) = E\{[x(t) - \hat{x}(t)]^T [x(t) - \hat{x}(t)]\}$. It follows that $\text{trace}(Y_o^{-1})$ is a measure of the average estimate covariance of the system [65].

B. JOINTLY CONTROLLABLE AND OBSERVABLE DIRECTIONS

Balanced realization theory for stable linear systems introduced by [66] provides additional tools for understanding the energy flow properties of a dynamical system. In particular, one can quantify the joint controllability and observability of a system that has been transformed into balanced coordinates $\tilde{x} = T_h x$, where $\{\hat{t}_i\}$ denote the columns of T_h^{-1}. In these new coordinates, the controllability and observability Gramians (Eqns. 4 and 5) are equal and diagonal, $\tilde{X}_c = \tilde{Y}_o = \text{diag}(h_1, \cdots, h_n)$ The Hankel singular values (HSVs), computed as the square roots of the eigenvalues of the product of the Gramians,

$$h_i = \sqrt{\lambda_i(Y_o X_c)}, \tag{8}$$

rank the joint controllability/observability of the directions $\hat{t}_i$ in original coordinates. In particular, directions with small h_i correspond to directions in state space that are simultaneously difficult to reach and observe. We define $\bar{h} = \max_i\{h_i\}$ as the maximum HSV and $\underline{h} = \min_i\{h_i\}$ as the minimum HSV, respectively.

Equations (6) and (7) cannot be used to compute Gramians for unstable systems directly, as they may have no solution or multiple solutions, and solutions are not positive (semi)definite. Instead, an extension to the unstable case was provided in [33], which showed that the Hankel singular values for an unstable system without eigenvalues on the imaginary axis can be computed as the union of the HSVs for the partitioned stable and unstable subsystems using the following partitioning:

$$\left(\begin{array}{c|c} TAT^{-1} & TB \\ \hline CT^{-1} & 0 \end{array}\right) = \left(\begin{array}{cc|c} A_s & 0 & B_s \\ 0 & A_u & B_u \\ \hline C_s & C_u & 0 \end{array}\right) \tag{9}$$

Let $G_s = (A_s, B_s, C_s)$ and $G_u = (A_u, B_u, C_u)$ be the stable and unstable subsystems, respectively. Then, the HSVs of $G = (A, B, C)$ can be computed as the union of the HSVs of G_s and G_u. The HSVs of G_u are equivalent to the HSVs of $G_u^* := (-A_u, B_u, C_u)$, and hence can be calculated using (6) and (7) since G_u^* is stable.

C. CONNECTIONS TO CLOSED LOOP PERFORMANCE AND ROBUSTNESS

1) MIMO SYSTEM DEFINITIONS

The Multi-Input Multi-Output (MIMO) block diagram shown in Fig. 1A is composed of plant $G(s) = (A, B, C)$ and controller $K(s)$. For $\Delta(s) = 0$, We define the closed-loop sensitivity transfer function $S_o = (I + GK)^{-1}$ as the map from exogenous inputs $r, n, d \in \mathbb{R}^m$ to the error signal $e \in \mathbb{R}^m$,

$$e = S_o(r - n - d). \tag{10}$$

We also define the closed-loop input demand transfer function $KS_o = K(I + GK)^{-1}$ as the map from exogenous inputs to the controlled input $u \in \mathbb{R}^p$,

$$u = KS_o(r - n - d). \tag{11}$$

The worst-case $L_2[0, \infty) \rightarrow L_2[0, \infty)$ or energy gain of the open or closed-loop transfer functions are captured using the infinity norm, which is the maximum singular value over frequency, i.e.,

$$\|G(s)\|_\infty = \sup_\omega \frac{\|y\|_2}{\|u\|_2} = \sup_\omega \bar{\sigma}[G(j\omega)]. \tag{12}$$

2) CLOSED LOOP DESIGN CONSIDERATIONS

The sensitivity function S_o is primarily associated with tracking performance and output disturbance/noise attenuation, so to minimize error e, its gain $\bar{\sigma}(S_o)$ should be small in the frequency range where the reference demand r, disturbances d or measurement noise n have content. The input demand function KS_o represents control energy and is associated with

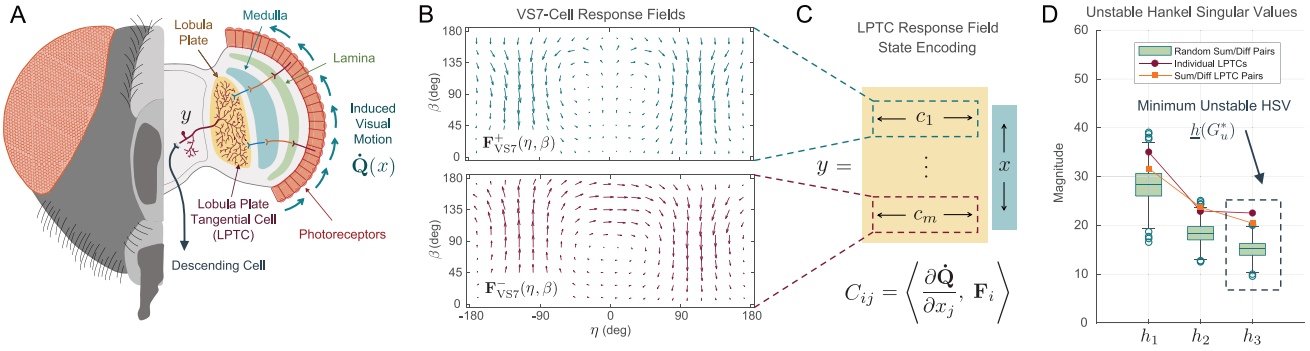

FIGURE 2. Sensorimotor convergence in the blowfly visual system. (A) Lobula Plate Tangential Cells (LPTCs) respond to wide-field optic flow, forming the output layer of the insect motion vision system. (B) Characterization of the LPTCs' response fields, such as the combined left and right VS7-cell response field displayed here, reveals that their local preferred directions closely match the optic flow associated with specific combinations of self-motion. (C) Representation of the output equation $y = Cx$, where the rows $\{c_i\}$ of the output matrix C capture the encoding of the rigid body state x for a given LPTC response field $\mathbf{F}_i$.(D) Hankel singular values for the unstable partition of the blowfly system compared to equivalent systems with randomly generated C matrices.

actuator saturation. Hence, to avoid large control signals at the plant input due to r, d or n, the gain $\bar{\sigma}(KS_o)$ should be small in the frequency ranges where these signals have content.

The input demand KS_o has additional constraints at low and high frequencies that shape closed-loop performance (Fig. 1B). At high frequencies where $\bar{\sigma}(GK) \ll 1$, we have $\bar{\sigma}(KS_o) \approx \bar{\sigma}(K)$. Therefore, to avoid large control signals due to high frequency content in disturbances or measurement noise, the controller gain $\bar{\sigma}(K)$ should be small. At low frequencies where $\bar{\sigma}(GK) \gg 1$, we have $\bar{\sigma}(KS_o) \approx 1/\underline{\sigma}(G)$. Note that this constraint on actuator saturation is a limitation set by the open-loop plant and cannot be influenced by control design, and therefore is one clear area where co-tuning of sensing, actuation, and dynamics can provide a significant benefit.

3) ROBUSTNESS

$\Delta(s)$ represents an appropriately dimensioned unstructured additive perturbation transfer function matrix (Fig. 1) which generates the family of uncertain plants

$$G_p(s) = \{G(s) + \Delta(s) \mid \Delta(s) \text{ unstructured}\}. \tag{13}$$

We say that the controller K robustly stabilizes (RS) the closed-loop system if it stabilizes every plant in G_p. For the additive perturbation shown, the small gain theorem is applied to generate the following necessary and sufficient result: if $\|\Delta\|_\infty \leq \varepsilon$, then

$$\text{RS} \iff \|KS_o\|_\infty < \frac{1}{\varepsilon}. \tag{14}$$

Therefore, the smaller the gain of the input demand $\bar{\sigma}(KS_o)$, the larger the perturbation $\bar{\sigma}(\Delta)$ the closed-loop system can tolerate.

Additionally, Glover [62] has shown that the minimum input demand to robustly stabilize the closed-loop system in Fig. 1A is directly related to the Hankel singular values of the open-loop system. In particular, there exists a single feedback controller K that stabilizes the set of plants $G_p = G + \Delta$ for all $\Delta < \varepsilon$ if and only if the minimum Hankel singular value of the unstable partition of the open-loop system satisfies $\underline{h}(G_u) \geq \varepsilon$. Therefore we have

$$\min_K \|KS_o\|_\infty = \frac{1}{\underline{h}(G_u)}. \tag{15}$$

This result is of particular interest as it connects the robustness property of the closed-loop system directly to an open-loop characteristic of the plant, which could be optimized through the co-tuning of sensing, actuation, and dynamics.

V. DIRECTIONAL OPTIMIZATION OF THE STATE SPACE C MATRIX

In this section we present two convex optimizations for the state space C matrix each of which maximizes one metric of joint controllability/observability based on HSVs. These optimizations tune the directions in state space which are encoded in the C matrix rows, and are formulated as semidefinite programs (SDPs) with linear matrix inequality (LMI) constraints. The first optimization minimizes the control energy required to stabilize an unstable system. The second optimization can be used for either stable or unstable systems, and minimizes the control energy required to achieve a prescribed system response speed. In Section VI-A we provide a method for realizing these directionally tuned C matrices using distributed sensing.

A. MOTIVATION

The visual system of the blowfly is an illustrative example of the principle of sensorimotor convergence, as shown in Fig. 2A. Neurons called Lobula Plate Tangential Cells (LPTCs) that respond to wide-field optic flow stimuli form the output layer of each optic lobe [67]. Measured response fields of individual LPTCs (Fig. 2B) indicate a strong dependence on self-motion parameters [4], [68]. A linearized matched filter approximation [5], [14], which assumes each output is the normalized projection of the induced visual motion, or optic flow $\dot{\mathbf{Q}}$, due to the insect's translational

and rotational self-motion onto its measured response field $\mathbf{F}_i$, is used to generate an output model $y = Cx$ (Fig. 2C). Rows of the associated C matrix, which can be composed from (i) individual left or right hemisphere response fields, or (ii) bilaterally summed and differenced response fields, correspond to the specific state encoding for each cell type.

Output models described above can then be paired with empirically parameterized A and B matrices for blowfly flight dynamics [17] to form open-loop systems $G = (A, B, C)$. In Fig. 2D, the Hankel singular values of the unstable partitions for each system are plotted against the HSVs for systems where the associated A and B matrices are paired with 1,000 randomly generated C matrices with normalized rows. The minimum unstable Hankel singular value $\underline{h}(G_u)$ for the biological ground truth is at the upper end of the distribution of the randomly generated systems. As this quantity is directly related to robustness and actuator saturation properties of the closed-loop system, it serves as a potentially useful choice of objective function. In the following, we leverage this conclusion regarding the minimum unstable HSV as the basis for an optimization framework which seeks to synthesize directions in state space for the C matrix to match sensory characteristics to the actuation and dynamics of a system.

B. UNSTABLE SYSTEMS: MAXIMIZING THE SMALLEST UNSTABLE HANKEL SINGULAR VALUE

In this case we consider unstable LTI state space systems $G = (A, B, C)$ and seek to maximize the smallest unstable HSV, which minimizes the smallest achievable value of $\|KS_o\|_\infty$ for all possible controllers. As shown in Section IV-C, this minimizes the control energy required to stabilize an unstable system, and maximizes the closed-loop robustness to additive unstructured uncertainty of the plant.

To compute the unstable HSVs, we (i) generate the transformation T that partitions the system into stable and unstable subsystems $G_s = (A_s, B_s, C_s)$ and $G_u = (A_u, B_u, C_u)$, respectively (9), then (ii) solve the Lyapunov equations in (6) and (7) for the reflected (stable) system $G_u^* = [-A_u, B_u, C_u]$. In the following it is useful to partition the transformation T in (9) such that

$$T = \begin{bmatrix} T_s \\ T_u \end{bmatrix}, \quad C = C_s T_s + C_u T_u, \tag{16}$$

and similarly partition its inverse $S = T^{-1}$ as

$$S = [\, S_s \;\; S_u \,], \quad C[\, S_s \;\; S_u \,] = [\, C_s \;\; C_u \,]. \tag{17}$$

For the optimization objectives we will consider, and likely others of interest, we must decide how to constrain the size of C. Since we are interested in finding the optimal state space directions to sense, and identifying corresponding sensitivity patterns, it makes sense to normalize either the rows of C or the sensitivity patterns themselves. We look here at synthesizing a C matrix with normed rows, that is, $c_i^T c_i = 1$ for each row c_i of C. While the HSVs themselves are invariant under coordinate transformations, normalization of C in different coordinate systems will not result in the same HSVs. In Section VI-A, we describe how to synthesize normalized sensitivity patterns.

We formalize the optimization problem described above as the following:

Proposition 1: Given a state space system (A, B), optimizing the directions in state space of the rows of the state space C matrix to minimize the achievable lower bound $\min_K \|KS_o\|_\infty$, is equivalent to the optimization problem:

$$\begin{aligned} \mathcal{A}: \quad & \max_C \min_i \; h_i(A_u, B_u, C_u) \\ & \text{s.t. } c_i^T c_i = 1 \quad \forall\, i = 1, \cdots, m \end{aligned} \tag{18}$$

where (A_u, B_u, C_u) is the unstable partition of the system, as shown in (9), T is the corresponding transformation, $C = [\, C_s \; C_u \,]T$, and $\{c_i^T\}$ are the rows of C.

Proof: This follows directly from [62]. □

Here we present an SDP with LMI constraints that solves the optimization problem presented above.

Theorem 2: The optimization problem $\mathcal{A}$ is equivalent to the following SDP posed as an LMI problem,

$$\mathcal{B}: \left(\underline{h}^\star(G_u)\right)^2 = \begin{cases} \min\limits_{Q,R,\rho} \rho \quad \text{s.t.} \\ Q > 0, R \geq 0 \\ -A_u^T Q + -Q A_u + R \geq 0 \\ \text{trace}(P^T R P) \leq 1 \\ X_{c,u}^{-1} \leq \rho Q \end{cases}$$
$$C^\star = U \Sigma V^T \tag{19}$$

where $X_{c,u}$ is the solution to (6) for $(-A_u, B_u)$, and

$$\begin{aligned} SVD(mP^T R P) &= V \Sigma^2 V^T \\ P &= T_u (I - T_s^T (T_s T_s^T)^{-1} T_s) \\ U &= \mathcal{U}(\Sigma) \end{aligned}$$

where m is the number of non-zero singular values of R, $\mathcal{U}$ denotes Algorithm 1, and T_s and T_u are the partitioning of T in (16).

The proof for Theorem (19) is provided in Appendix A.

Algorithm 1 is needed to map the optimization variable $R = C^T C$ to a set of normalized rows of C or sensitivity patterns. It takes as input a diagonal matrix of singular values, Σ and produces a unitary matrix U denoted $U = \mathcal{U}(\Sigma)$. Such a unitary matrix U which maps $C^T C$ to a C matrix with normalized rows always exists as shown in the proof for Theorem 2 in Appendix A.

C. MINIMIZING CONTROL EFFORT FOR STABLE AND UNSTABLE SYSTEMS

For the second optimization, which can be applied to stable or unstable LTI systems, we minimize the smallest achievable value of $\|KS_o\|_\infty$ for all possible controllers that produce a prescribed closed-loop speed of response, defined as being

Algorithm 1 $U = \mathcal{U}(\Sigma)$

$U \leftarrow \text{zeros}(m)$
$U(1,:) \leftarrow \mathbf{r_1} = \left[\frac{1}{\sqrt{m}}, \ldots, \frac{1}{\sqrt{m}}\right]$
for $i = 2 : m$ **do**
$r_i \leftarrow \min_{\mathbf{r_i}} \left|\mathbf{r_i}\Sigma^2\mathbf{r_i}^T - 1\right|$ s.t. $\begin{cases} \mathbf{r_i}\mathbf{r_i}^T = 1 \\ U\mathbf{r_i}^T = [0, \ldots, 0]^T \end{cases}$
$U(i,:) \leftarrow \mathbf{r_i}$
end for

faster than $e^{-\alpha t}$ for a specified α. We do this by maximizing the minimum unstable HSV of a modified system.

For certain stable systems, one could consider maximizing the minimum HSV of the full system using SDP $\mathcal{A}$ in (2), in order to maximize the joint controllability-observability. Related approaches are taken in [54], which maximize the minimum singular values of the controllability and observability Gramians over the actuator and sensor selection options, respectively. However, for many systems we have little leverage to increase the smallest stable HSV using the C matrix, resulting in substantial sensing required for small increases in this value. Therefore, we propose a different approach that maximizes the minimum HSV for a portion of the system whose HSVs set a lower bound on the control energy required to achieve a desired closed-loop bandwidth. This optimization can be applied to stable or unstable systems.

In [69], the authors demonstrate that the problem of synthesizing a controller to obtain a certain speed of response can be reformulated as a stabilization problem for a modified system. The minimum unstable HSV of this modified system then determines the control effort required to meet this performance requirement. We reiterate their result here, then apply our methods to minimize this lower bound on control energy by optimizing the directions encoded in C.

Let us assume the system $G = (A, B, C)$ has a desired closed-loop response faster than $e^{-\alpha t}$, where $\alpha > 0$. As this requirement corresponds to restricting closed-loop poles to the left of $s = -\alpha$ on the complex plane, this can be converted to a stabilization problem for the system $G' = (A', B, C)$, $A' = A + \alpha I$. Then, the minimum control effort required to achieve the performance metric is:

$$\min_K \|KS_o'\|_\infty = \frac{1}{\underline{h}(G_u')}, \tag{20}$$

where $G_u'(s) = (A_u', B_u, C_u)$ is the antistable partition of G' as given in Section IV-B [69].

Therefore, given a desired closed-loop bandwidth α, we can optimize C to minimize the achievable lower limit on the required control energy over all possible controllers.

Theorem 3: Let $G(s) = (A, B)$ be a plant for which we aim to synthesize a C matrix and controller K such that the closed-loop poles of $G_{cl}(s) = C[sI - (A + BK)]^{-1}B$ are to the left of $s = -\alpha$ in the complex plane. Let $G' = (A', B, C)$, $A' = A + \alpha I$. Then, the SDP $\mathcal{B}$ applied to G' produces a C matrix that minimizes the control effort (20) over all possible controllers. Finally, a controller $K(s)$ that achieves this lower bound is found using the synthesis approach in [62] to produce $K(s')$, $K(s) = K(s' - \alpha)$.

Proof: This result follows directly from [62] and [69], and Theorem 2. □

VI. FRAMEWORK FOR OPTIMIZING DISTRIBUTED SENSING SYSTEMS

In Section V, we provided SDPs for optimizing state space C matrices for two optimization objectives. Now we describe a framework for realizing an optimized C matrix using distributed sensing. This can be used together with the previous contribution, or separately, to implement a different desirable C matrix.

First, we provide a framework for processing signals from distributed sensing systems, inspired by the pooling approach described in Section V-A. We integrate this framework with conventional state space modeling such that traditional linear systems tools and theory can be applied. We then modify the optimization problems presented in Section V to synthesize spatial sensitivity patterns which provide a method to implement the optimized sensing system.

A. DISTRIBUTED SENSING APPROACH

We consider a dynamical system which is able to sense some spatially varying vector or scalar field, which we call the measurement field and denote g. The measurement field depends on the system state, x, and the spatial location, γ, at which g is measured. We denote the spatial region over which g can be sensed as Γ, and $\gamma \in \Gamma$. The dimension of the measurement field at a given state and spatial location is denoted as q.

We define the following function space:

$$\begin{aligned} \mathcal{F} &:= \mathcal{L}^2(\Gamma, \mathbb{R}^q) \\ &= \{f : \Gamma \to \mathbb{R}^q \mid \int_\Gamma \|f(\gamma)\|^2 d\gamma < \infty\} \end{aligned} \tag{21}$$

With inner product:

$$\langle f,\ g\rangle_{\mathcal{F}} := \int_\Gamma \langle f(\gamma),\ g(\gamma)\rangle\, d\gamma \tag{22}$$

(where $\langle \cdot,\ \cdot \rangle$ denotes the inner product on $\mathbb{R}^q$) and norm:

$$\|f\|_{\mathcal{F}} := \left[\int_\Gamma \|f(\gamma)\|^2 d\gamma\right]^{1/2}. \tag{23}$$

We assume that:

1) The spatial domain Γ is bounded
2) Given any state x in the state space, $g(x, \cdot) \in \mathcal{F}$
3) The measurement field g does not depend on the control input u, i.e., in the linearization $D = 0$.

To process spatially varying measurements, we use the pooling approach described in Section V-A, which we model as in [15]:

$$y_i = \langle \phi_i(\gamma),\ g(x, \gamma)\rangle_{\mathcal{F}} \tag{24}$$

where $\{\phi_i\}_{i=1}^m$ is a set of sensitivity patterns, $\phi_i \in \mathcal{F}$, which we aim to design. The system compares each sensitivity pattern ϕ_i to the actual sensory input g measured by the sensors, to produce a measurement y_i. We aim to optimize these sensitivity patterns to improve the closed-loop performance of the system.

B. STATE SPACE FORMULATION

We consider the following system model, for which we will optimize the sensitivity patterns $\{\phi_i\}_{i=1}^m$:

$$\begin{cases} \dot{x} = f(x,u) \\ y_i = \langle \phi_i(\gamma),\ g(x,\gamma) \rangle_{\mathcal{F}} \end{cases} \tag{25}$$

where $x \in \mathbb{R}^n$ is the system state, $u \in \mathbb{R}^r$ is the control input, $\{y_i\}_{i=1}^m \in \mathbb{R}^m$ are the measurements, and $f : \mathbb{R}^n \times \mathbb{R}^r \to \mathbb{R}^n$ is the nonlinear dynamics function.

We linearize system (25) about equilibrium state $(\bar{x}, \bar{u})$:

$$\begin{cases} \delta\dot{x} = \dfrac{\partial}{\partial x} f(x,u)\Big|_{(\bar{x},\bar{u})} \delta x + \dfrac{\partial}{\partial u} f(x,u)\Big|_{(\bar{x},\bar{u})} \delta u \\ y_i = \left\langle \phi_i(\gamma),\ \dfrac{\partial}{\partial x} g(x,\gamma)\Big|_{\bar{x}} \right\rangle_{\mathcal{F}} \delta x \end{cases} \tag{26}$$

where the expression for y_i applies the linearity of the inner product. Using the standard state space notation and renaming δx and δu as x and u:

$$\begin{cases} \dot{x} = Ax + Bu \\ y_i = c_i^T x \end{cases} \tag{27}$$

where and $A \in \mathbb{R}^{n\times n}$, $B \in \mathbb{R}^{n\times r}$ and c_i is a row of the state space C matrix, $C \in \mathbb{R}^{m\times n}$:

$$c_i^T = \langle \phi_i(\gamma),\ J(\gamma) \rangle_{\mathcal{F}} \in \mathbb{R}^{1\times m} \tag{28}$$

$$J(\gamma) := \frac{\partial}{\partial x} g(x,\gamma)\Big|_{\bar{x}} \in \mathcal{F} \times \cdots \times \mathcal{F} \tag{29}$$

We aim to optimize the sensitivity patterns $\{\phi_i\}$ to improve the desired performance of the system. We will do this by optimizing the state space C matrix, as in Section V, and then finding corresponding sensitivity patterns $\{\phi_i\}$. To do this, we must approximate $\{\phi_i\}$ in a finite-dimensional space.

First, we choose an orthonormal basis for the function space $\mathcal{F}$, which will depend on the problem. We then choose a finite subset of these basis functions to form a finite-dimensional approximation to this basis, denoted $\mathcal{B} := \{\mathcal{B}_k\}_{k=1}^N$. We denote the projection of some $X(\gamma) \in \mathcal{F}$ onto $\mathcal{B}$:

$$[X]_{\mathcal{B}} = \begin{bmatrix} \langle X(\gamma),\ B_1(\gamma) \rangle_{\mathcal{F}} \\ \vdots \\ \langle X(\gamma),\ B_N(\gamma) \rangle_{\mathcal{F}} \end{bmatrix} \in \mathbb{R}^N \tag{30}$$

The amount of information lost through the choice of $\mathcal{B}$ can be quantified using the following procedure:

1) Compute the norm $\|\cdot\|_{\mathcal{F}}$ of each element

$$J_j(\gamma) = \frac{\partial}{\partial x_j} g(x,\gamma)\Big|_{\bar{x}} \tag{31}$$

2) Project each of the elements J_j, onto $\mathcal{B}$:

$$[J_j]_{\mathcal{B}} := [\langle J_j(\gamma),\ B_1(\gamma) \rangle_{\mathcal{F}}, \ldots, \langle J_j(\gamma),\ B_N(\gamma) \rangle_{\mathcal{F}}]^T \tag{32}$$

3) Compute the 2-norm of each element's projection, i.e. take the 2-norm of the coefficients of $[J_j]_{\mathcal{B}}$
4) Ensure the ratio of these norms is close to 1 for all j:

$$\frac{\|[J_j]_{\mathcal{B}}\|}{\|J_j(\gamma)\|_{\mathcal{F}}} \leq 1 \tag{33}$$

These ratios quantify the signal energy of each element of J that is preserved using the finite set of basis functions.

With this finite dimensional approximation, each row of C is produced by the following matrix multiplication:

$$c_i = [\phi_i]_{\mathcal{B}}^T \left[\frac{\partial g}{\partial x}\Big|_{\bar{x}} \right]_{\mathcal{B}} \tag{34}$$

The output matrix C is then given by:

$$C = \Phi_{\mathcal{B}} J_{\mathcal{B}}, \tag{35}$$

$$\Phi_{\mathcal{B}} = \begin{bmatrix} [\phi_1]_{\mathcal{B}}^T \\ [\phi_2]_{\mathcal{B}}^T \\ \vdots \\ [\phi_m]_{\mathcal{B}}^T \end{bmatrix} \in \mathbb{R}^{m\times N}, \qquad J_{\mathcal{B}} := \left[\frac{\partial g}{\partial x}\Big|_{\bar{x}} \right]_{\mathcal{B}} \in \mathbb{R}^{N\times n} \tag{36}$$

In the remainder, the subscript $\mathcal{B}$ will be dropped.

C. REALIZABILITY

As discussed in Section VI-B, the Jacobian J encodes information about the mapping between ϕ_i and c_i. In particular, J can be used to ensure that a sensing system is physically realizable. This can be written as a condition on Φ:

$$\phi_i \in \mathcal{R}(J) \quad \forall i = 1, \ldots, m \tag{37}$$

The condition that a state space C matrix is physically realizable is equivalent to

$$c_i \in \mathcal{R}(J^T) \quad \forall i = 1, \ldots, m \tag{38}$$

This is equivalent to the condition

$$CP_J = C, \quad P_J := J^\dagger J \tag{39}$$

This is used in optimization $\mathcal{D}$ to derive the value of P_r, which ensures the resulting optimized C matrix is realizable.

The computation of P_r requires the definition of the operator $\cap(\cdot, \cdot)$. This operator takes as input two projections, and produces a projection onto the intersection of the rowspaces of the arguments. Let P_1 and P_2 be square projection matrices in $\mathbb{R}^{n\times n}$. Then $\cap(P_1, P_2)$ is found as [70]:

$$\cap(P_1, P_2) = USV^T \tag{40}$$

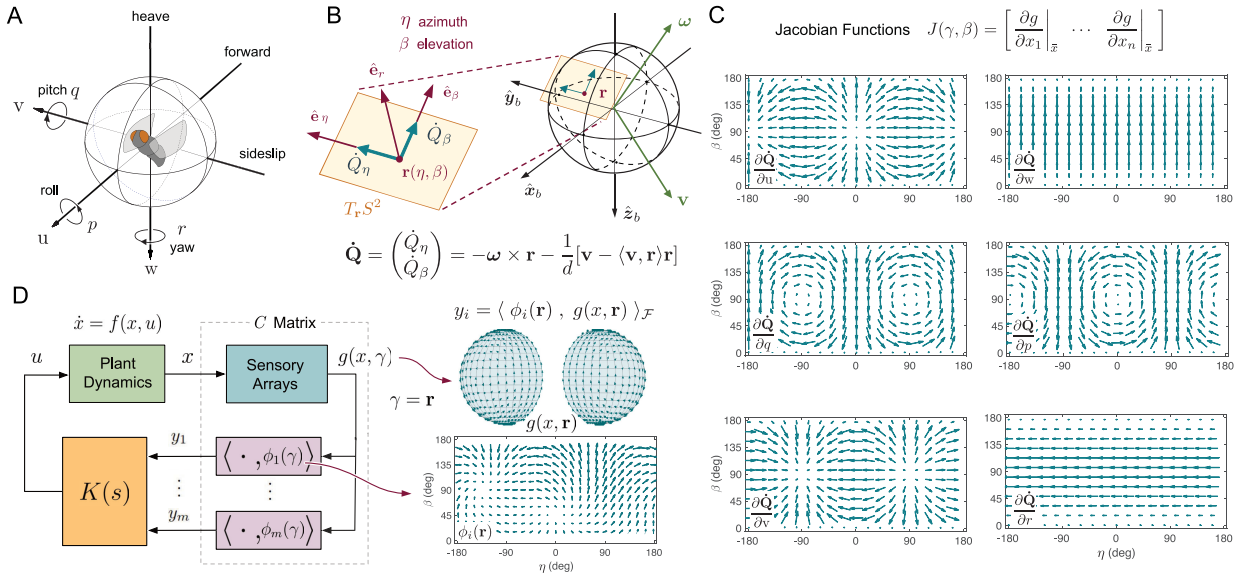

FIGURE 3. Framework for optic-flow based distributed sensory processing and control. (A) Each lobula plate tangential cell (LPTC) of the fly's motion vision system responds preferentially to some specific combination of rotational (roll, pitch, yaw) and translational (forward, sideslip, heave) self-motion. (B) The azimuth and elevation components of the optic flow vector are the projected relative rotational and translational velocities of visual contrasts or objects in the environment into the tangent space of the imaging surface, modelled here as a sphere. The translational contribution at each viewing direction $\mathbf{r} = (\eta, \beta)$ is inversely scaled by the distance $d(\eta, \beta)$ from the imaging surface to the nearest object in the environment. (C) Jacobian functions for optic flow relative to rigid body states x. The Jacobian functions not shown are equal to zero. (D) MIMO feedback architecture; outputs y_i are generated by projecting the instantaneous optic flow estimates onto sensitivity functions ϕ_i and are fed to a dynamic controller K.

where

$$U\Sigma V^T = \mathrm{SVD}(P_1P_2), \quad \Sigma = \begin{bmatrix} \sigma_1 & & \\ & \ddots & \\ & & \sigma_n \end{bmatrix}$$

$$S = \begin{bmatrix} s_1 & & \\ & \ddots & \\ & & s_n \end{bmatrix}, \quad s_i = \begin{cases} 1, & \sigma_i = 1 \\ 0, & \text{otherwise} \end{cases} \tag{41}$$

D. OPTIC FLOW ON THE SPHERE

As an example, we consider optic flow generated on a spherical imaging surface due to 6-DOF motion in a 3D environment (Fig. 3A,B). The sensing region is taken as the 2-sphere $\Gamma = S^2$, where an optic flow vector $\dot{\mathbf{Q}} = [\dot{Q}_\eta \ \dot{Q}_\beta]^T \in \mathbb{R}^2$ is defined at each spatial location $\gamma = \mathbf{r}$, parameterized using the azimuth η and elevation β angles as

$$\mathbf{r}(\eta, \beta) = [\cos\eta \sin\beta \quad \sin\eta \sin\beta \quad \cos\beta]^T. \tag{42}$$

We assume that the $(\eta, \beta) = (0, 90°)$ axis points along the body $\hat{\boldsymbol{x}}_b$ axis. Hence, the function space of interest is $\mathcal{F} = \mathcal{L}^2(S^2, \mathbb{R}^2)$, with measurement field $g(x, \gamma) = \dot{\mathbf{Q}}(x, \mathbf{r})$ and sensitivity patterns $\phi_i(\gamma)$ corresponding to LPTC receptive fields $\mathbf{F}_i(\mathbf{r})$, yielding outputs

$$y_i = \langle \phi_i(\gamma), g(x, \gamma) \rangle_{\mathcal{F}} = \int_{S^2} \mathbf{F}_i(\mathbf{r}) \cdot \dot{\mathbf{Q}}(x, \mathbf{r}) \, d\Omega, \tag{43}$$

as defined in Fig. 3D. Here Ω is the solid angle on the sphere and the inner product $\mathbf{F}_i \cdot \dot{\mathbf{Q}}$ is calculated locally at each spatial location $\mathbf{r}(\eta, \beta)$ on the sphere.

E. OPTIMIZING SENSITIVITY PATTERNS

Here we adapt SDP $\mathcal{B}$ (19) to the problem of synthesizing sensitivity patterns for a distributed sensing system which maximize the minimum unstable HSV. This modified optimization accounts for constraints on the states the system is able to sense through the Jacobian J. Additionally, a constraint is modified to ensure that the sensitivity patterns themselves are normalized, rather than the rows of the C matrix.

Theorem 4: The optimization problem:

$$\begin{aligned} &\max_{\Phi} \min_{i} \ h_i(A_u, B_u, C_u(\Phi)) \\ \mathcal{C}: \quad &C_u(\Phi) = \Phi J S_u \\ &\text{s.t. } \phi_i^T \phi_i = 1 \quad \forall\, i = 1, \cdots, m \end{aligned} \tag{44}$$

where (A_u, B_u, C_u) is the unstable partition of the system, as shown in (9) with the corresponding S_u in (17), is equivalent to the following SDP posed as an LMI problem,

$$\mathcal{D}: \quad \left(\underline{h}^\star(G_u)\right)^2 = \begin{cases} \min \rho \quad \text{s.t.} \\ Q > 0, R \geq 0 \\ -A_u^T Q + -QA_u + P_r^T R P_r \geq 0 \\ \mathrm{trace}(P_n^T R P_n) \leq 1 \\ X_{c,u}^{-1} \leq \rho Q \end{cases}$$

$$P_r := P_J + P_{s\cap J^\perp}, \quad P_J := J^\dagger J$$

$$P_{s\cap J^\perp} := \cap(P_s, P_J^\perp), \quad P_s := T_s^T (T_s T_s^T)^\dagger T_s$$

$$P_c := T_u P_J (I - J^\dagger (J^\dagger)^T (T_s J^\dagger (J^\dagger)^T T_s^T)^\dagger P_{s\cap J})$$

$$P_{s\cap J} := \cap(P_s, P_J)$$

$$P_n := P_c U_J \Sigma_J^{1/2}, \quad SVD(J^\dagger J) = U_J \begin{bmatrix} \Sigma_J \\ 0 \end{bmatrix} V_J^T \tag{45}$$

where $X_{c,u}$ is the solution to (6) for $(-A_u, B_u)$, the operator $\cap(\cdot, \cdot)$ is the projection onto the intersection of the rowspaces of the arguments (see Section VI-C), and the resulting R is mapped to Φ via:

$$\Phi = \bar{U} \Sigma V^T, \quad U \Sigma V^T = SVD(\sqrt{m} R^{1/2} P_c J^\dagger) \tag{46}$$

where m is the number of nonzero singular values of the optimized R and $\bar{U}$ is generated by Algorithm 1 with input Σ.

The proof for Theorem 4 is provided in Appendix A.

VII. MULTIVARIABLE CONTROLLER SYNTHESIS

To complete the framework introduced in this paper, we discuss two controller synthesis approaches that highlight and leverage the properties of open-loop systems that have been optimized using the techniques described in Sections V and VI.

A. MAXIMALLY ROBUST CONTROL

As discussed in Section IV-C3, the minimum unstable HSV of a system determines the lowest possible $\|KS_o\|_\infty$ over all possible K, for the feedback configuration shown in Fig. 3D. In [62], Corollaries 6.1 and 6.2 provide a formulation for the controller which achieves this lower bound on $\|KS_o\|_\infty$ for a given system. This controller synthesis approach illustrates the effect of our sensing design methodology on the achievable performance of the system.

The following adapts the synthesis method for a maximally robust controller given in [62]. Note that some of the source notation has been changed for consistency.

Theorem 5: (Adapted from Glover [62]) Let the state space system $G(s) = (A, B, C)$ be partitioned into stable and antistable parts, $G_s(s) = (A_s, B_s, C_s)$ and $G_u(s) = (A_u, B_u, C_u)$, respectively, such that $G = G_s + G_u$.

Let G_u be a balanced realization with balanced Gramians:

$$\Sigma = \begin{bmatrix} \Sigma_1 & 0 \\ 0 & \varepsilon I \end{bmatrix}; \quad \Sigma_1 - \varepsilon I > 0 \tag{47}$$

such that ε is the smallest HSV. Let (A_u, B_u, C_u) be partitioned compatibly with Σ into (A_{u1}, B_{u1}, C_{u1}) and (A_{u2}, B_{u2}, C_{u2}). Let

$$K = K_2 (I + G_s K_2)^{-1} \tag{48}$$

where

$$\begin{aligned} K_2 &= \tilde{D} + \tilde{C}(sI - \tilde{A})^{-1}\tilde{B} \\ \tilde{D} &= \varepsilon^{-1} U^* \\ \tilde{C} &= \varepsilon^{-1} U^* C_{21} \Sigma_1 + B_{21}^* \\ \tilde{B} &= -\tilde{\Gamma}^{-1}(\varepsilon^{-1} \Sigma_1 B_{21} U^* + C_{21}^*) \\ \tilde{A} &= -A_{21}^* I + \tilde{B} C_{21} \Sigma_1 \\ U &= -(C_{22}^T)^\dagger B_{22} \\ \tilde{\Gamma} &= \Sigma_1^2 - \varepsilon^2 I \end{aligned} \tag{49}$$

Then K is a maximally robust controller for G, such that $\|KS_o\|_\infty = \frac{1}{\varepsilon}$.

Proof: This result follows directly from Lemma 6.1 and Corollaries 6.1 and 6.2 in [62]. □

The application of Theorem 5 yields a maximally robust controller K that achieves the lower bound on the input demand transfer function KS_o. While useful from both comparative and validation perspectives, this controller has limited practical utility as it does not allow the designer to specify additional performance requirements such as tracking error or disturbance attenuation, as determined by the sensitivity transfer function S_o. To increase flexibility in the design process, one can consider the mixed-sensitivity synthesis approach outlined in the next section.

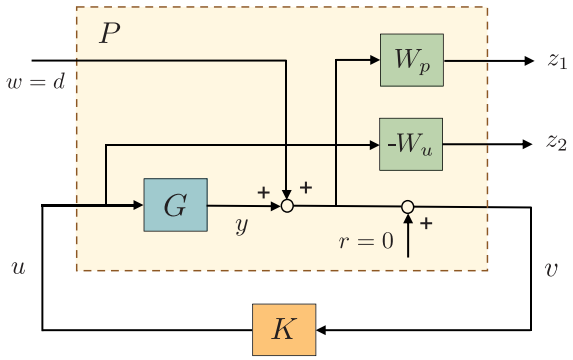

FIGURE 4. H_∞ *S/KS* **mixed sensitivity block diagram in regulator form. The generalized plant *P* is composed of plant *G*, controller *K*, and performance and actuator weighting functions W_p and W_u.**

B. MIXED SENSITIVITY H_∞ CONTROL

Consider the general feedback configuration with generalized plant P and controller K shown in Fig. 4 where w are exogenous signals such as references or disturbances, z are the controlled variables, v are any signals the controller has access to such as errors, and u are the plant inputs. If the plant transfer function P is partitioned as

$$\begin{pmatrix} z_1 \\ z_2 \\ v \end{pmatrix} = \left(\begin{array}{c|c} P_{11} & P_{12} \\ \hline P_{21} & P_{22} \end{array}\right) \begin{pmatrix} w \\ u \end{pmatrix}, \tag{50}$$

we can express the closed-loop transfer function from w to $z = [z_1^T \; z_2^T]^T$ as,

$$\begin{aligned} z &= [P_{11} + P_{12} K (I - P_{22} K)^{-1} P_{21}]\, w \\ &= F_l(P, K)\, w. \end{aligned} \tag{51}$$

In the standard H_∞ synthesis approach [71], one seeks to select a stable controller K that minimizes the effect of the exogenous signals w on the controlled outputs z though the following optimization problem:

$$\inf_K \|F_l(P, K)\|_\infty = \inf_K \max_\omega \bar{\sigma}[F_l(P, K)(j\omega)]. \tag{52}$$

For our application, we consider the S/KS mixed sensitivity case, which corresponds to the block diagram in Fig. 4. This encodes the following objectives: (i) attenuation of low-frequency disturbances at the plant output, (ii) minimization of high-frequency actuator gain, and (iii) robust stability to additive uncertainty at high frequencies. The first requires that $\bar{\sigma}(S_o)$ be small at low frequencies, and the second and third require that $\bar{\sigma}(KS_o)$ be small at high frequencies.

To allow for specification of low- and high-frequency performance bounds on S_o and KS_o, frequency-dependent weighting functions $W_p(s)$ and $W_u(s)$ are introduced as shown in Fig. 4. The corresponding generalized plant is given by

$$P = \left(\begin{array}{c|c} P_{11} & P_{12} \\ \hline P_{21} & P_{22} \end{array}\right) = \left(\begin{array}{c|c} W_p & W_pG \\ \hline 0 & -W_u \\ \hline -I & -G \end{array}\right), \tag{53}$$

with controlled variables $z_1 = W_pS_ow$ and $z_2 = W_uKS_ow$. This particular choice of feedback structure results in the H_∞ S/KS mixed sensitivity optimization problem

$$\inf_K \|F_l(P,K)\|_\infty = \inf_K \left\| \begin{bmatrix} W_pS_o \\ W_uKS_o \end{bmatrix} \right\|. \tag{54}$$

This formulation now allows for a trade-off between minimization of actuator effort and robustness (KS_o) and disturbance rejection and tracking capability (S_o), in contrast to the maximally robust controller from the previous section.

The mixed-sensitivity H_∞ control synthesis was performed using the dynamic output H_∞ SDP provided in [72] and implemented using YALMIP [73].

VIII. EXAMPLES

In the following examples we apply the SDPs from Theorem 3 and Theorem 5 to synthesize C matrices and their associated sensitivity patterns for several systems. We also apply optimal controller synthesis techniques from Section VII to highlight the closed-loop benefits of sensing characteristics that are tuned to the actuation and dynamics properties of the system.

A. BLOWFLY CALLIPHORA

We use SDP $\mathcal{B}$ (19) to synthesize a C matrix with three rows (Appendix B-A) and generate the corresponding sensitivity patterns ϕ_1, ϕ_2, and ϕ_3. The optimal C matrix (Appendix B-A) has nonzero components corresponding to the pitch and roll angles, which are not observable. However, these components are small, and setting them to zero reduces the minimum unstable HSV from 9.38 to 9.31, a difference of less than 1%. Note that SDP $\mathcal{D}$ accounts for this realizability condition automatically. For this problem, the optimal value of the optimization variable R has two nonzero singular values, but we choose to map it to three (linearly dependent) C matrix rows for comparison with the three heterolateral V1, V2, and Vx cells.

For comparison purposes, we select the outputs formed from the left and right heterolateral V1, V2, and Vx Lobula Plate Tangential Cell (LPTC) response fields (denoted $\mathbf{F}^-_{V1}$, $\mathbf{F}^-_{V2}$, and $\mathbf{F}^+_{Vx}$, respectively). These cells were shown to have strong correlations with the most controllable/observable directions [17], which suggests a connection to the Hankel singular values.

Fig. 5A shows the resulting Hankel singular values for the unstable partition for the *Calliphora* system with (i) asymmetric V1 and V2 and symmetric Vx LPTC combined response fields, (ii) outputs synthesized using SDP $\mathcal{B}$, and (iii) 1000 randomly generated 3×8 C matrices with normalized rows chosen from a uniform distribution on $\mathbb{R}^8$. Fig. 5B-C compares the corresponding measured response fields to the sensitivity patterns resulting from the optimization. It is clear that the *Calliphora* and synthesized C matrices result in a larger minimum unstable HSV and a larger Hankel norm compared to the randomly generated systems. Additionally, the synthesized C matrix provides a 42.7% increase in the minimum unstable HSV over the biological system. Note that in the *Calliphora* combined left and right heterolateral response fields we have introduced a symmetry constraint as in [17], whereas the optimized sensitivity patterns have introduced a coupling in the longitudinal (symmetric) and lateral (asymmetric) dynamics through the pitch rate q and roll rate p states. This could explain, at least in part, the gap in the resulting minimum unstable HSV between the LPTC response fields and the optimal (synthesized) sensitivity patterns.

B. MICRO-HELICOPTERS

In this section we consider two micro-helicopters, the flybarless Walkera V100D04 and its flybarred counterpart, the Walkera CB100. The flybarless version is inherently unstable in pitch and roll, while the flybarred version is equipped with a Bell stabilizer bar that enforces rotational stability and alters the character of the dynamics. LTI models composed of state space A and B matrices for their respective flight and actuator dynamics about hover were empirically identified using time and frequency domain methods in [74]. The heave w and yaw rate r states were assumed to be decoupled, resulting in the state and input vectors

$$x = [\ \phi\ \ \theta\ \ p\ \ q\ \ a\ \ b\ \ c\ \ d\ \ u\ \ v\ ]^T \tag{55}$$

$$u = [\ \delta_{\text{lat}}\ \ \delta_{\text{lon}}\ ]^T, \tag{56}$$

where ϕ and θ are the roll and pitch attitude states, p and q are the roll and pitch rates, and the forward and lateral velocities are u and v, in SI units. The states a and b represent the rotor flapping dynamics (both helicopters), and c and d are the flybar dynamics (flybarred helicoper only). Inputs δ_{lat} and δ_{lon} represent the lateral and longitudinal swashplate inputs.

We assume each micro-helicopter is equipped with 4π steradian optic flow sensing and synthesize optic flow sensitivity patterns utilizing the optimizations developed in Section VI-E to micro-helicopter flight dynamics with and without a flybar installed. The optic flow Jacobian J was computed using spherical harmonic basis functions of up to

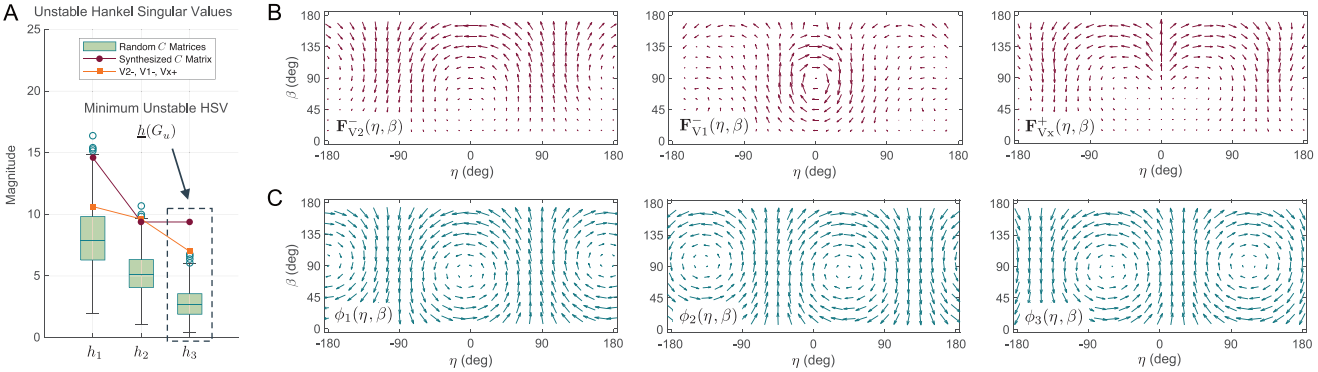

FIGURE 5. Blowfly *Calliphora* output C matrix comparisons. (A) Hankel singular values from the unstable partition for (i) the C matrix corresponding to the V2$^-$, V1$^-$, and Vx$^+$ measured response fields, (ii) the C matrix synthesized with LMI $\mathcal{B}$ (19) using the Calliphora A and B matrices, and (iii) 1000 random C matrices with normalized rows chosen from a uniform distribution. (B) Measured response fields for the asymmetric V2 and V1, and symmetric Vx Lobula Plate Tangential Cells. (C) Sensitivity patterns $\{\phi_i\}$ for the three rows of the synthesized C matrix.

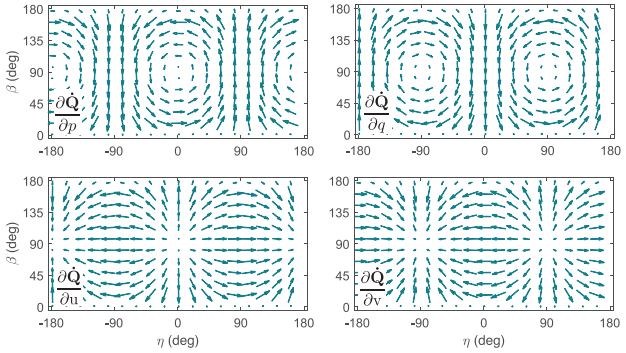

FIGURE 6. Optic flow Jacobians for the hover reference flight condition for the micro-helicopter observable states.

8^{th} degree for the hover reference flight condition and is shown for the four observable states $\{p, q, \text{u}, \text{v}\}$ in Fig. 6. Then, maximally robust and optimal H_∞ controllers were synthesized to provide disturbance rejection capability about the hover equilibrium. The authors chose not to focus on a specific set of requirements for this application, therefore the weighting functions W_p and W_u used in the H_∞ mixed synthesis were developed to demonstrate an appropriate balance between controller effort and tracking performance.

1) FLYBARRED MICRO-HELICOPTER

In this example we first apply SDP $\mathcal{D}$ (45) to synthesize optic flow sensitivity patterns ϕ_1^h and ϕ_2^h (Fig. 7C) and the associated output matrix C_1 using state space A and B matrices for the flybarred micro-helicopter. As the nominal dynamics are stable, we consider the shifted system with the prescribed speed of response $\alpha = .75$ (Section V-C). We denote this optimized open-loop system as $G_1 = (A, B, C_1)$.

For comparison, we generate a second set of optic flow sensitivity patterns ϕ_1^o and ϕ_2^o (Fig. 7D) by maximizing the smallest eigenvalue of the observability Gramian. This is analogous to the more traditional approach to distributed sensing optimization, which seeks to minimize some metric of the state estimate error covariance [29]. We implement this optimization by solving the following SDP with LMI constraints:

$$\begin{cases} \min \rho \quad \text{s.t.} \\ Q > 0, R > 0 \\ -A^T Q + -QA + P_r^T R P_r \geq 0 \\ \text{trace}(P_n^T R P_n) \leq m \\ I \leq \rho Q \end{cases} \tag{57}$$

$$P_r := J^\dagger J, \quad P_n := P_r J^\dagger \tag{58}$$

where R is mapped to sensitivity patterns in the same way as for SDP $\mathcal{D}$. The optimization produces four rows of the C matrix, and the relative gain array was used to down-select to the best two rows to match the input dimensions of the plant. We denote the associated output matrix as C_2, and the open-loop system as $G_2 = (A, B, C_2)$.

The structure of the synthesized patterns and the associated states that are encoded by the C matrices (Appendix B-B) reveal the result of applying SDP $\mathcal{D}$. The eigenvectors of the slowest open-loop poles of the plant, $s_{1,2} = -0.4160 \pm 1.1304j$ and $s_{3,4} = -0.6017 \pm 0.8111j$, are dominated by the u and v states, respectively. It is clear that the patterns ϕ_1^h and ϕ_2^h in Fig. 7C are a combination of these states, and are primarily translational in nature. The patterns synthesized using the observability metric, on the other hand, aim to make the least observable states, p and q, more observable, though their measurement may have little relevance to the closed-loop dynamics.

To explore the closed-loop implications of the sensory tunings, the maximally robust controller and the S/KS mixed-sensitivity H_∞ optimal controller (Section VII) were synthesized for the systems $G_1 = (A, B, C_1)$ and $G_2 = (A, B, C_2)$. The H_∞ performance and actuator weights were chosen as $W_p(s) = w_p(s)I$ and $W_u(s) = w_u(s)I$ (Appendix B). This yields controllers $K_1(s')$ and $K_2(s')$ in terms of the shifted

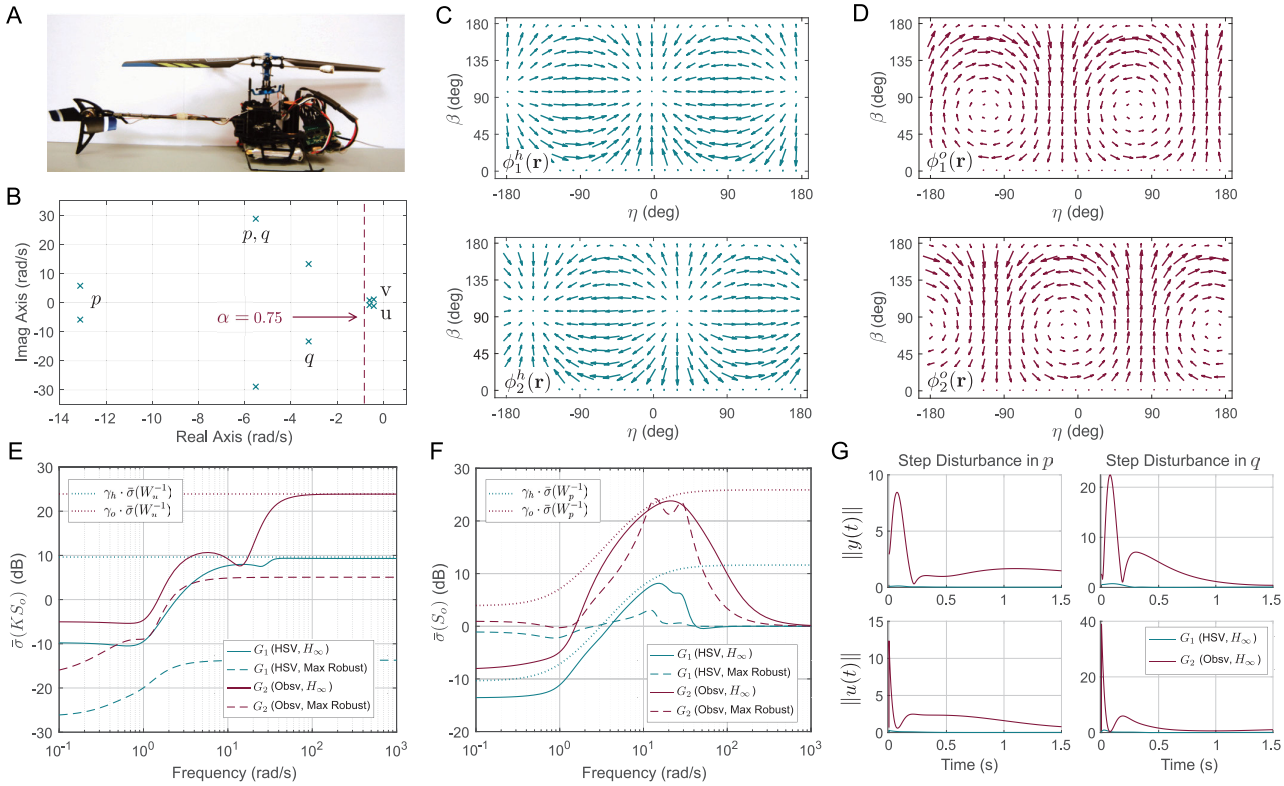

FIGURE 7. Optic flow sensing and control optimization applied to a flybarred micro-helicopter. (A) Walkera CB100 micro-heli with flybar installed. (B) The eigenstructure of the A matrix is plotted along with dominant eigenvector states. (C) Sensitivity patterns resulting from maximizing the minumum unstable HSV for the $\alpha = .75$ case. (D) Sensitivity patterns resulting from maximizing the minimum singular value of the observability Gramian. (E-F) Closed-loop frequency response of the transfer functions KS_o and S_o with the max robust and S/KS mixed sensitivity H_∞ controllers. (G) Magnitudes of the output y and actuator input u signals for a step disturbance input in roll rate p for the optimized HSVs (G_1) and the maximized observability (G_2) systems.

variable s', and must be shifted back by substituting $s' = s+\alpha$ into the transfer functions.

In Fig. 7E-F, we plot the maximum singular value of the KS_o and S_o closed-loop transfer functions. It is clear that the max robust controller minimizes $\|KS_o\|_\infty$, while the H_∞ controller allows for additional design flexibility to push down $\bar{\sigma}(S_o)$ at lower frequencies to improve tracking and disturbance rejection performance at the expense of increasing $\|KS_o\|_\infty$. Comparing the HSV-optimized and the observability-optimized systems G_1 and G_2, the optimized HSV system provides the lowest worst-case actuator effort to achieve the same speed of response set by the parameter $\alpha = .75$, provides the maximum robustness to additive uncertainty, and exhibits improved disturbance rejection capability, as verified by the step responses plotted in Fig. 7G.

2) FLYBARLESS MICRO-HELICOPTER

The effect of removing the flybar is revealed in the eigenstructure plot in Fig. 8B, where a pair of unstable complex-valued poles appear in the right half plane at $s_{1,2} = 0.9126 \pm 2.2232j$. The associated eigenvectors are now composed of the pitch rate q and roll rate p states, along with a contribution from the forward velocity u. The eigenvector content is similar for the stable complex pole pair at $s_{3,4} = -1.5567 \pm 2.4754j$, hence the slowest open-loop poles have shifted from being translational to rotational in nature.

SDP $\mathcal{D}$ (45) was applied to the A and B matrices empirically identified in [74] representing the flight dynamics of this system about hover. The associated optic flow sensitivity patterns ϕ_1^h and ϕ_2^h for the synthesized C matrix (Appendix B-C) are shown in Fig. 8C. The spatial structure of these patterns is now a combination of rotational and translational velocity, reflective of the dynamic character of the dominant low-frequency poles of the open-loop system.

Closed-loop properties were also investigated by implementing the max robust and S/KS mixed sensitivity H_∞ controllers as in the previous example. The H_∞ performance and actuator weights were chosen as $W_p(s) = w_p(s)I$ and $W_u(s) = w_u(s)I$ (Appendix B). In Fig. 8D, we plot $\bar{\sigma}(KS_o)$ where the desired closed-loop speed of response specification is varied from $\alpha = 0$ to $\alpha = 4$. It is clear that increasing the desired response speed increases the minimum actuator effort $\|KS_o\|_\infty$ required to stabilize the system and reduces robustness to additive uncertainty. The additional design flexibility of the mixed sensitivity H_∞ approach is reflected in the $\bar{\sigma}(KS_o)$ and $\bar{\sigma}(S_o)$ frequency response plots in Fig. 8E,F where a moderate increase in actuator effort (4.5 dB) is traded for significant disturbance rejection performance (41.37 dB).

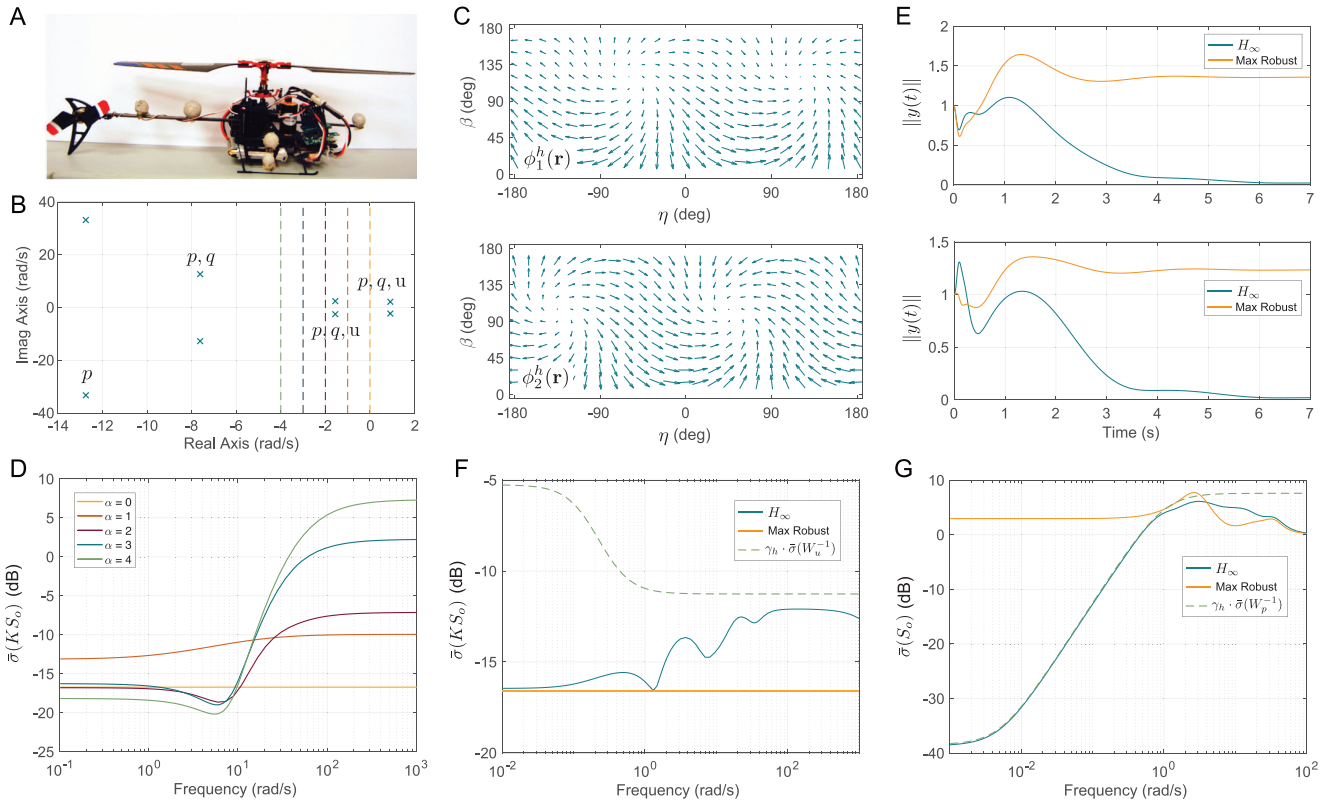

FIGURE 8. Optic flow sensing and control optimization applied to a flybarless micro-helicopter. (A) Walkera V100D04 flybarless micro-heli. (B) The eigenstructure of the A matrix is plotted along with dominant eigenvector states. (C) Synthesized optic flow patterns for the $\alpha = 0$ case. (D) Closed-loop frequency response with the max robust controller of the transfer function KS_o for the $\alpha = 0, 1, 2, 3, 4$ systems. (E-G) Closed-loop output response $\|y(t)\|$ to a step in the first and second disturbance d components and frequency response of the transfer functions KS_o and S_o for the max robust and the S/KS mixed sensitivity H_∞ controllers for the $\alpha = 0$ case.

This is verified by the responses for the magnitude of the output $\|y(t)\|$ for step inputs in each of the output disturbance directions $d \in \mathbb{R}^2$.

IX. DISCUSSION

This article leverages insights from recently discovered connections in blowfly flight physics and physiology as the basis for an optimization framework to synthesize spatial sensitivity patterns for systems equipped with distributed sensor arrays. Within the proposed framework, we presented two novel semidefinite programs (SDPs) with linear matrix inequality (LMI) constraints which maximize the smallest unstable Hankel singular value (HSV) of the system, a coordinate-invariant metric which minimizes the actuator effort and maximizes the achievable robustness of an LTI system. A maximally robust controller synthesis method was adapted from previous work, which provides a validation tool, and the H_∞ controller formulation presented allows for a trade-off between minimization of actuator effort and robustness versus disturbance rejection and tracking capability, in contrast to the maximally robust controller.

The first SDP (19) synthesizes a state space C matrix with directionally optimized rows, while the second SDP (45) synthesizes spatial sensitivity patterns that provide a method to realize an optimized C matrix using a distributed sensor array. Both SDPs can be applied to unstable systems, in particular to the portion of the system whose HSVs set a lower bound on the control energy required to achieve a desired closed-loop bandwidth. To extend this to stable systems, we incorporated an operator that shifts the eigenvalues of the A matrix, which is equivalent to enforcing a minimum speed of response constraint.

Applying this approach to empirically parameterized *Calliphora* flight dynamics shows correlation between the optimized sensitivity patterns and the true response fields measured in the animal. Of particular note, the optimization generates sensitivity patterns that introduce coupling between the longitudinal (symmetric) and lateral (asymmetric) partitions of the dynamics, which is consistent with the observation that outputs composed of LPTC response fields from individual (left or right) hemispheres have a slightly larger minimum unstable HSV, compared to pairwise summed or differenced response fields, which enforce bilateral symmetry.

Sensitivity patterns were also synthesized for flybarred and flybarless micro-helicopter flight dynamics. The addition of the flybar enforces rotational stability, and significantly alters the character of the dynamics. The synthesized sensitivity

patterns capture this difference, as they reflect the states in the dominant (slowest) poles of the dynamics. In particular, the flybarred patterns are tuned to forward and lateral velocity, whereas the flybarless patterns are tuned to a combination of pitch and roll rates with a forward velocity component (Figs. 7C and 8C). As a point of comparison with traditional methods, a separate SDP with LMI constraints was fomulated to generate sensitivity patterns for the flybarred (stable) micro-helicopter that maximize the smallest eigenvalue of the observability Gramian. The resulting patterns were composed primarily of the pitch and roll rate states.

Disturbance rejection feedback loops were closed on both micro-helicopters using both a maximally robust controller and a mixed sensitivity H_∞ optimal controller. Note the observability-based synthesis could not be applied to the flybarless micro-helicopter as those dynamics are unstable. The benefits of the HSV-optimized system over the observability-optimized system were readily apparent upon analysis of the respective closed-loop behaviors on the flybarred micro-helicopter. In particular, the HSV-optimized approach provides the lowest worst-case actuator effort to achieve the same speed of response, provides the maximum robustness to additive uncertainty, and exhibits improved disturbance rejection capability, demonstrating a successful transition of a biological principle that improves the engineered system.

The novelty of this problem indicates the potential for many improvements on and extensions to this work. One improvement would include a modified metric that includes the impact of amplitude scaling. For instance, multiplying the output matrix C by a constant which scales the HSVs by the same value, or duplicating a row of the C matrix which scales the HSVs by a factor of $\sqrt{2}$. Neither of these modifications actually improves system performance, and in the case of amplitude scaling, may amplify signal-to-noise issues. In this work we avoid this problem by synthesizing normalized and linearly independent sensitivity patterns (or C matrix rows), but we can still only make fair comparisons between sensing systems with the same number of sensitivity patterns or C matrix rows.

One straightforward extension is to modify the optimizations introduced here to the problem of sensor selection using the minimum unstable HSV metric, potentially using mixed-integer semidefinite programs (MISDPs). The performance of a spatially distributed sensor array using synthesized sensitivity patterns could then provide an upper bound on the performance of a sparse sensor array. Other work could include the development of additional coordinate-independent optimization objectives for sensitivity pattern synthesis, which are linked to closed-loop system performance. Finally, these spatial sensitivity patterns could be extended to include a temporal component [75], further improving potential performance and noise rejection capabilities, or combined with alternative feedback architectures for disturbance rejection, such as [76] and [77].

As engineered systems become increasingly interconnected, integrated, and high-dimensional, new design principles will be required to achieve optimal dynamic performance. Approaches that allow for simultaneous specification of sensors, actuators, dynamics, and closed-loop performance will be essential to achieve this goal. Bio-inspired principles, such as the maximization of the smallest unstable Hankel singular value explored in this article, show immediate promise for applications such as highly agile morphing vehicles, continuum-type platforms involving flexible bodies and soft actuators or robots, cyber-physical systems, flow control systems, resource management systems, communication systems, and power networks.

APPENDIX A PROOFS AND SUPPORTING RESULTS

Lemma 1: Let the positive semi-definite matrix $R \in \mathcal{P}^n$ satisfy $\text{trace}(R) = m$, *where $m \in \mathbb{N}$ and m greater than or equal to the number of nonzero singular values of R. Then, there exists a matrix $C \in \mathbb{R}^{m\times n}$ which satisfies $R = C^T C$, and $\mathbf{c}_i^T \mathbf{c}_i = 1 \quad \forall\, i \in \{1, \cdots, m\}$, where $\mathbf{c}_i^T$ are the rows of C.*

Proof: We prove that there exists such a C by constructing the matrix U described above, such that $C = U\Sigma V^T$.

Using the following notation:

$\mathbf{u}_i$: jth column of U
u_{ij}: element of U in the ith row, jth column
$\mathbf{v}_i$: jth row of V
σ_j: jth diagonal element of Σ
$\mathbf{c}_i^T$: ith row of C
$\mathbf{e}_i$: unit vector with 1 in the ith entry and zeros elsewhere
$\mathbf{r}_i$: ith row of U

Then,

$$C = \sum_{j=1}^{n} \sigma_j \mathbf{u}_j \mathbf{v}_j^T$$

and

$$\mathbf{c}_i^T = \sum_{j=1}^{n} \sigma_j \mathbf{e}_i^T \mathbf{u}_j \mathbf{v}_j^T = \sum_{j=1}^{n} \sigma_j u_{ij} \mathbf{v}_j^T$$

The constraint that C must have normalized rows is equivalent to

$$\text{trace}(\mathbf{c}_i \mathbf{c}_i^T) = 1 \; \forall i$$

Hence

$$\begin{aligned} \text{trace}\left(\sum_{j=1}^{n} \sigma_j^2 u_{ij}^2 \mathbf{v}_j \mathbf{v}_j^T\right) &= \sum_{j=1}^{n} \sigma_j^2 u_{ij}^2 \,\text{trace}(\mathbf{v}_j \mathbf{v}_j^T) \\ &= \sum_{j=1}^{n} \sigma_j^2 u_{ij}^2 = 1. \end{aligned} \tag{59}$$

Therefore the rows $\{\mathbf{r}_i\}$ must satisfy:

1) $\mathbf{r}_i \mathbf{r}_j^T = 0 \quad \forall i \neq j$
2) $\|\mathbf{r}_i\| = 1 \quad \forall i$
3) $\sum_{j=1}^{n} \sigma_j^2 u_{ij}^2 = 1$

The first two constraints come from U being unitary. The third constraint is equivalent to restricting each $\mathbf{r}_i$ to the surface of a hyper-ellipsoid in $\mathbb{R}^m$ with semi-axis lengths $\frac{1}{\sigma_1}, \ldots, \frac{1}{\sigma_n}$. Combining the second and third requirements implies that each $\mathbf{r}_i$ should lie on the intersection of this hyper-ellipsoid and the unit sphere.

The condition $\text{trace}(R) = m$ ensures that this intersection is nonempty since:

$$\text{trace}(R) = m \quad \Longleftrightarrow \quad \sum_{j=1}^{n} \sigma_j^2 = m$$

The trivial case is all $\sigma_j = 1$, in which case any unitary U suffices. In the nontrivial case, some $\sigma_j > 1$, and some $\sigma_j < 1$. Therefore the hyper-ellipsoid with semi-axis lengths $\frac{1}{\sigma_1}, \ldots, \frac{1}{\sigma_n}$ will always intersect the unit sphere. The existence of an orthonormal set of vectors $\{\mathbf{r}_i\}_{i=1}^m$ that lie in this intersection is shown in Lemma 2.

Algorithm 1 constructs such a set starting with $\mathbf{r_1} = \left[\frac{1}{\sqrt{m}}, \ldots, \frac{1}{\sqrt{m}}\right]$ which is always a solution. $m-1$ orthonormal solutions are then constructed.

□

Lemma 2: Given an ellipsoid $\mathcal{E}_m$ in $\mathbb{R}^m$ with semi-axis lengths $\frac{1}{\sigma_1}, \ldots, \frac{1}{\sigma_n}$ represented by $\mathbf{v}^T E_m \mathbf{v} = 1$ where $\mathbf{v} \in \mathbb{R}^m$ and $E_m \in \mathbb{R}^{m\times m}$,

$$E_m = \begin{bmatrix} \sigma_1^2 & \mathbf{0} & \cdots & \mathbf{0} \\ \mathbf{0} & \sigma_2^2 & \cdots & \mathbf{0} \\ \vdots & \vdots & \ddots & \vdots \\ \mathbf{0} & \mathbf{0} & \cdots & \sigma_m^2 \end{bmatrix}, \tag{60}$$

and $\text{trace}(E_m) = m$, there exists a set of orthonormal vectors $\{\mathbf{v}_i\}_{i=1}^m$ that lie on the intersection of $\mathcal{E}_m$ and the unit sphere in $\mathbb{R}^m$.

Proof: The vector $\left[\frac{1}{\sqrt{m}}, \ldots, \frac{1}{\sqrt{m}}\right]^T$ is always in this intersection, therefore we choose this for $\mathbf{v}_1$. The intersection of $\mathcal{E}_m$ and the orthogonal subspace to the span of $\mathbf{v}_1$ is another ellipsoid $\mathcal{E}_{m-1} \in \mathbb{R}^{m-1}$.

The next step is therefore to show that the intersection of $\mathcal{E}_{m-1}$ and the unit sphere in $\mathbb{R}^{m-1}$ is non-empty, so that a $\mathbf{v}_2$ may be selected from this intersection.

Consider the projection P_1 onto the orthogonal subspace to $\text{span}\{\mathbf{v}_1\}$:

$$P_1 = I - \mathbf{v}_1\mathbf{v}_1^T = \frac{1}{m}\begin{bmatrix} m-1 & -1 & \cdots & -1 \\ -1 & m-1 & \cdots & -1 \\ \vdots & & \ddots & \vdots \\ -1 & \cdots & -1 & m-1 \end{bmatrix} \tag{61}$$

Then, $\mathcal{E}_{m-1}$ can be represented by $E_{m-1} = P_1 E_m P_1^T$, $\mathbf{v}^T P_1 E_m P_1^T \mathbf{v} = 1$. The sum of the eigenvalues of E_{m-1} can be found via the trace:

$$\sum_{i=1}^{m} \lambda_i(E_{m-1}) = \text{trace}(P_1 E_m P_1^T) = \sum_{i=1}^{m} \sigma_i^2 \,\text{trace}(\mathbf{p}_{1,i}\mathbf{p}_{1,i}^T) \tag{62}$$

where $\mathbf{p}_{1,i}$ are the columns of P_1. The reader can verify that $\text{trace}(\mathbf{p}_{1,i}\mathbf{p}_{1,i}^T) = \frac{m-1}{m} \quad \forall i$, and therefore

$$\sum_{i=1}^{m} \lambda_i(E_{m-1}) = m - 1. \tag{63}$$

Therefore, using the same reasoning as for $\mathcal{E}_m$, $\mathcal{E}_{m-1}$ intersects with the unit sphere in $\mathbb{R}^{m-1}$. After transforming $\mathcal{E}_{m-1}$ into coordinates in the subspace orthogonal to the span of $\mathbf{v}_1$, such that E_{m-1} is diagonalized, we can choose $[\mathbf{v}_2]_2 = \left[\frac{1}{\sqrt{m-1}}, \ldots, \frac{1}{\sqrt{m-1}}\right]^T$ ($\mathbf{v}_2$ in this new coordinate system $[\,\cdot\,]_2$) and this process can be repeated.

At the $m-1$th iteration, $[\mathbf{v}_{m-1}]_{m-1} = \left[\frac{1}{\sqrt{2}}, \frac{1}{\sqrt{2}}\right]^T$ and $[\mathbf{v}_m]_{m-1} = \left[\frac{1}{\sqrt{2}}, -\frac{1}{\sqrt{2}}\right]^T$, and this process is complete. □

Here we provide the proof for Theorem 2.

Theorem 2 *The optimization problem $\mathcal{A}$ is equivalent to the following SDP with LMI constraints,*

$$\mathcal{B}: \ \left(\underline{h}^\star(G_u)\right)^2 = \begin{cases} \min\limits_{Q,R,\rho} \ \rho \quad \text{s.t.} \\ Q > 0, R \geq 0 \\ -A_u^T Q + -QA_u + R \geq 0 \\ \text{trace}(P^T R P) \leq m \\ X_{c,u}^{-1} \leq \rho Q \end{cases} \tag{64}$$

$$C^\star = U\Sigma V^T \tag{65}$$

where $X_{c,u}$ is the solution to (6) for $(-A_u, B_u)$, and

$$\begin{aligned} \text{SVD}(P^T R P) &= V\Sigma^2 V^T \\ P &= T_u(I - T_s^T(T_s T_s^T)^{-1} T_s) \\ U &= \mathcal{U}(\Sigma) \end{aligned} \tag{66}$$

where $\mathcal{U}$ denotes Algorithm 1, and T_s and T_u are the partitioning of T in (16).

Proof: First we prove that the optimization problem $\mathcal{A}$ is equivalent to

$$\begin{aligned} &\max_{C_s, C_u} \ \min_i \ h_i(A_u, B_u, C_u) \\ &\text{s.t.} \begin{cases} \|C'\|_F^2 = m \\ C' = C_s T_s + C_u T_u \end{cases} \\ &C^\star = U\Sigma V^T, \ \text{SVD}(C') = U'\Sigma V^T, \ U = \mathcal{U}(\Sigma) \end{aligned} \tag{67}$$

This is the result of replacing the optimization variable C with its partitioned components C_s and C_u. The constraint $c_i^T c_i = 1$ requiring C to have normalized rows, is replaced by the condition $\|C'\|_F^2 = m$ on the intermediary variable C'. This follows from Lemma 1 which ensures the existence of a unitary U which maps C' to a C with normalized rows.

Next, the condition $\|C'\|_F^2 = m$ can be relaxed to $\|C'\|_F^2 \leq m$. Consider a C' such that $\|C'\|_F^2 < m$. Then there exists an $\alpha > 1$, $\tilde{C} = \alpha C'$, $\tilde{C}_u = \alpha C_u$. Then $\min\limits_i \ h_i(A_u, B_u, \tilde{C}_u) > \min\limits_i \ h_i(A_u, B_u, C_u)$. Hence for an optimal C', $\|C'\|_F^2 = m$.

Now we find the optimal value of C_s as a function of the optimal value of C_u. Note that C_s does not directly affect the unstable HSVs, but only indirectly through its influence on the constraint $\|C'\|_F^2 \leq m$. Let $C' = C_sT_s + C_uT_u$, and let $\tilde{C}_s$ be such that $\|\tilde{C}\|_F^2 < \|C'\|_F^2$ where $\tilde{C} = \tilde{C}_sT_s + C_uT_u$. Then there exists an $\alpha > 1$, $\tilde{C} = \alpha C'$, $\tilde{C}_u = \alpha C_u$. Then $\min_i h_i(A_u, B_u, \tilde{C}_u) > \min_i h_i(A_u, B_u, C_u)$. Therefore, the optimal choice of C_s is $\operatorname{argmin}_{C_s} \|C'\|_F^2$.

The optimal choice for C_s can be found in terms of C_u. Let $\tilde{P}$ be the projection onto the nullspace of T_s ($\tilde{P} : \mathbb{R}^n \to \text{Null}(T_s)$) and $\tilde{P}^\perp$ be the projection onto the rowspace of T_s ($\tilde{P}^\perp : \mathbb{R}^n \to \text{Ran}(T_s^T)$):

$$\begin{aligned} \tilde{P}^\perp &= T_s^T(T_sT_s^T)^{-1}T_s \\ \tilde{P} &= I - T_s^T(T_sT_s^T)^{-1}T_s \end{aligned} \tag{68}$$

Then, C' can be decomposed as:

$$C' = C_sT_s + C_uT_u(\tilde{P}^\perp + \tilde{P}) \tag{69}$$

and the choice of C_s that minimizes $\|C'\|_F$ is

$$C_sT_s = -C_uT_u\tilde{P}^\perp \tag{70}$$

and correspondingly

$$C' = C_uT_u\tilde{P}. \tag{71}$$

Thus our optimization $\mathcal{A}$ is equivalent to:

$$\max_{C_u} \min_i h_i(A_u, B_u, C_u) \quad \text{s.t.} \begin{cases} \|C_uP\|_F^2 \leq m \\ C = U\Sigma V^T,\ \text{SVD}(C_uP) = U'\Sigma V^T,\ U = \mathcal{U}(\Sigma) \end{cases} \tag{72}$$

Now, rewriting the objective as an eigenvalue minimization problem, minimizing the largest eigenvalue of the inverse of the product of the unstable observability and controllability Gramians, the optimization becomes:

$$\begin{cases} \min_{C_u} \rho \\ -A_u^TQ + -QA_u + C_u^TC_u = 0 \\ \|C_uP\|_F^2 \leq m \\ X_{c,u}^{-1} \leq \rho Q \end{cases} \tag{73}$$

$$C = U\Sigma V^T,\ \text{SVD}(C_uP) = U'\Sigma V^T,\ U = \mathcal{U}(\Sigma) \tag{74}$$

As this is non-linear in C_u we perform the substitution $R = C_u^TC_u$. Additionally, the number of non-zero singular values of R, and hence the number of linearly independent rows of C which R can be mapped to, is not known before running the optimization. Therefore the condition $\text{trace}(P^TRP) \leq m$ is replaced by $\text{trace}(P^TRP) \leq 1$, and the resulting optimal R is multiplied by m, the number of non-zero singular values of R.

Finally, we expand the feasible set of Q by relaxing the equality in (73) to an inequality, such that Q remains the observability Gramian for the optimal solution:

$$\begin{cases} \min \rho \\ Q > 0,\ R \geq 0 \\ -A_u^TQ + -QA_u + R \geq 0 \\ \text{trace}(P^TRP) \leq m \\ X_{c,u}^{-1} \leq \rho Q \end{cases}$$

$$C = U\Sigma V^T,\ \text{SVD}(C_uP) = U'\Sigma V^T,\ U = \mathcal{U}(\Sigma) \tag{75}$$

□

The following lemma is required for the proof of Theorem 4.

Lemma 3: Given matrices $A \in \mathbb{R}^{m\times n}$, $T \in \mathbb{R}^{p\times n}$, $M \in \mathcal{P}^n$, $M \geq 0$, then the solution $X^\star \in \mathbb{R}^{m\times p}$ to the following minimization

$$\min_X \mathcal{J}(X) \tag{76}$$

$$\mathcal{J}(X) = \text{trace}((XT + A)M(XT + A)^T) \tag{77}$$

is

$$X^\star = -AMT^T(TMT^T)^\dagger \tag{78}$$

Proof: First, note that for matrices $B \in \mathbb{R}^{m\times n}$ and $M \in \mathbb{R}^{n\times n}$,

$$\text{trace}(BMB^T) = \sum_{i=1}^m b_i^TMb_i, \quad B = \begin{bmatrix} \longleftarrow & b_1^T & \longrightarrow \\ & \vdots & \\ \longleftarrow & b_n^T & \longrightarrow \end{bmatrix} \tag{79}$$

Therefore the effect of each row of $(XT + A)$ on the objective is independent and each optimal row can be solved for individually:

$$\mathcal{J}(X) = \sum_{i=1}^m (x_i^TT + a_i^T)M(T^Tx_i + a_i) \tag{80}$$

where x_i^T and a_i^T are the rows of X and A, respectively.

$$\frac{\partial \mathcal{J}(X)}{\partial x_i} = 2(x_i^TT + a_i^T)MT^T \tag{81}$$

Setting this equal to zero:

$$x_i^T = -a_i^TMT^T(TMT^T)^\dagger \tag{82}$$

The Hessian at this value of x_i^T is $2TMT^T$ which is positive semi-definite due to the condition that $M \geq 0$. Therefore

$$X^\star = -AMT^T(TMT^T)^\dagger \tag{83}$$

This optimum is only unique when TMT^T is full rank. The general solution when TMT^T is not full rank is

$$X^\star = -AMT^T(TMT^T)^\dagger + \tilde{X}P_M^\perp \tag{84}$$

where $\tilde{X}$ is any matrix in $\mathbb{R}^{m\times p}$ and P_M is the projection onto the rowspace of M, $P_M^\perp = I - M(MM)^\dagger M$. □

Here we provide the proof for Theorem 4.

Theorem 4 *The optimization problem:*

$$\begin{aligned} &\max_{\Phi} \min_{i} \; h_i(A_u, B_u, C_u(\Phi)) \\ &\mathcal{C}: C_u(\Phi) = \Phi J S_u \\ &\quad \text{s.t. } \phi_i^T \phi_i = 1 \quad \forall\, i = 1, \cdots, m \end{aligned} \tag{85}$$

where (A_u, B_u, C_u) is the unstable partition of the system, as shown in (9) with the corresponding S_u in (17), is equivalent to the following SDP with LMI constraints,

$$\mathcal{D}: \quad \left(\underline{h}^\star(G_u)\right)^2 = \begin{cases} \min \rho \quad \text{s.t.} \\ Q > 0, R \geq 0 \\ -A_u^T Q + -Q A_u + P_r^T R P_r \geq 0 \\ \text{trace}(P_n^T R P_n) \leq m \\ X_{c,u}^{-1} \leq \rho Q \end{cases}$$

$$\begin{aligned} P_r &:= \Sigma_J V_J^T, \quad \text{SVD}(J S_u) = U_J \begin{bmatrix} \Sigma_J \\ 0 \end{bmatrix} V_J^T \\ P_n &:= P_r T_u (I - T_s^T (T_s T_s^T)^{-1} T_s) J^\dagger \end{aligned} \tag{86}$$

where $X_{c,u}$ is the solution to (6) for $(-A_u, B_u)$, and the resulting R is mapped to Φ via:

$$\Phi = \bar{U} \Sigma V^T, \quad U \Sigma V^T = \text{SVD}(R^{1/2} P_n) \tag{87}$$

where $\bar{U}$ is generated by Algorithm 1 with input Σ.

Proof: Most of this result follows from Theorem 2.

There are two changes to Theorem 2, the first is the substitution of R for $P_r^T R P_r$. The second is in the definition of P_n. These modifications arise from the realizablity of C and the optimal choice of the stable part of the C matrix, C_s. C_s does not affect the unstable HSVs directly, but does affect the size of the resulting sensitivity patterns. Therefore, as in the proof of Theorem 2, the optimum value of C_s must be found in terms of C_u.

C is decomposed as:

$$C = \bar{C}_s + \bar{C}_u, \quad \bar{C}_s = C_s T_s, \quad \bar{C}_u = C_u T_u \tag{88}$$

For the optimized C matrix to be realizable, that is, achievable using the prescribed sensory system, the following condition is required:

$$C = C P_J, \quad P_J = J^\dagger J \tag{89}$$

To ensure the partitioning of C into C_s and C_u is valid,

$$\bar{C}_s = \bar{C}_s P_s, \quad P_s = T_s^T (T_s T_s^T)^\dagger T_s \tag{90}$$

$$\bar{C}_u = \bar{C}_u P_u, \quad P_u = T_u^T (T_u T_u^T)^\dagger T_u \tag{91}$$

Using the decomposition of C, $\text{trace}(\Phi^T \Phi)$ can be written as:

$$\begin{aligned} &\text{trace}(\Phi^T \Phi) \\ &\quad = \text{trace}((J^\dagger)^T (C_s T_s + C_u T_u)^T (C_s T_s + C_u T_u) J^\dagger) \\ &\quad = \text{trace}((C_s T_s + C_u T_u) J^\dagger (J^\dagger)^T (C_s T_s + C_u T_u)^T) \end{aligned} \tag{92}$$

From Lemma 3, the choice of C_2 that minimizes $\text{trace}(\Phi^T \Phi)$ is

$$C_s^\star = -C_u T_u J^\dagger (J^\dagger)^T (T_s J^\dagger (J^\dagger)^T T_s^T)^\dagger + \tilde{C}_s P_J^\perp \tag{93}$$

To satisfy the realizability condition (89), and partitioning (90), $\tilde{C}_s$ must be

$$\tilde{C}_s = -C_u T_u \tag{94}$$

and the realizability projection P_r must be

$$P_r = P_J + P_{s \cap J^\perp} \tag{95}$$

where $P_{s \cap J^\perp}$ projects onto the intersection between the rowspaces of P_J and P_s and is computed as in Section VI-C. P_r ensures that

$$C_u T_u P_J^\perp = C_u T_u P_{s \cap J^\perp} \tag{96}$$

such that the following is acheivable:

$$C_s^\star T_s P_J^\perp = -C_u T_u P_J^\perp \tag{97}$$

Finally, to ensure realizablility (89) and valid partitioning (90),

$$C_s^\star = -C_u T_u J^\dagger (J^\dagger)^T (T_s J^\dagger (J^\dagger)^T T_s^T)^\dagger P_{s \cap J} - C_u T_u P_J^\perp \tag{98}$$

resulting in the following optimal C and Φ

$$\begin{aligned} C^\star &= C_s^\star T_s + C_u T_u \\ &= C_u T_u P_J (I - J^\dagger (J^\dagger)^T (T_s J^\dagger (J^\dagger)^T T_s^T)^\dagger P_{s \cap J}) \end{aligned} \tag{99}$$

$$\begin{aligned} \Phi^\star &= C_s^\star T_s + C_u T_u \\ &= C_u T_u P_J (I - J^\dagger (J^\dagger)^T (T_s J^\dagger (J^\dagger)^T T_s^T)^\dagger P_{s \cap J}) J^\dagger \end{aligned} \tag{100}$$

and the value of $\text{trace}(\Phi^T \Phi)$ is

$$\text{trace}(\Phi^T \Phi) = \text{trace}(P_n^T C_u^T C_u P_n) \tag{101}$$

$$P_n = T_u P_J (I - J^\dagger (J^\dagger)^T (T_s J^\dagger (J^\dagger)^T T_s^T)^\dagger P_{s \cap J}) J^\dagger \tag{102}$$

□

APPENDIX B EXAMPLE DATA

A. BLOWFLY CALLIPHORA

$$\begin{aligned} x &= [\text{u}, \text{w}, q, \theta, \text{v}, p, \phi, r]^T \quad \text{[SI units]} \\ \bar{x} &= [0, 0, 0, 0, 0, 0, 0.8509, 0, 0, 0, 0, 0]^T \end{aligned}$$

Optimal C matrix:

$$C = \begin{bmatrix} 0.0008 & 0.0039 & 0.1084 & 0.0051 & 0.0283 & 0.9795 & 0.0849 & 0.1443 \\ 0.0070 & 0.0329 & 0.9035 & 0.0423 & 0.0121 & 0.4190 & 0.0363 & 0.0617 \\ -0.0050 & -0.0234 & -0.6434 & -0.0301 & 0.0218 & 0.7533 & 0.0653 & 0.1110 \end{bmatrix}$$

Optimal C matrix with unobservable states removed:

$$C = \begin{bmatrix} 0.0008 & 0.0039 & 0.1084 & 0 & 0.0283 & 0.9795 & 0 & 0.1443 \\ 0.0070 & 0.0329 & 0.9035 & 0 & 0.0121 & 0.4190 & 0 & 0.0617 \\ -0.0050 & -0.0234 & -0.6434 & 0 & 0.0218 & 0.7533 & 0 & 0.1110 \end{bmatrix}$$

B. FLYBAR HELICOPTER

$$\begin{aligned} x &= [\phi, \theta, p, q, a, b, c, d, \text{u}, \text{v}]^T \quad \text{[SI units]} \\ \bar{x} &= [0, 0, 0, 0, 0, 0, 0, 0, 0, 0]^T \end{aligned}$$

C matrix maximizing the minimum unstable HSV:

$$C_1 = \begin{bmatrix} 0 & 0 & -0.0812 & -0.3930 & 0 & 0 & 0 & 0 & -2.882 & 0.1602 \\ 0 & 0 & 0.0433 & -0.4040 & 0 & 0 & 0 & 0 & -2.491 & -1.456 \end{bmatrix}$$

C matrix maximizing the observability of the least observable states:

$$C_2 = \begin{bmatrix} 0 & 0 & 1.044 & 2.618 & 0 & 0 & 0 & 0 & -0.6225 & 0.3992 \\ 0 & 0 & 2.746 & -0.6768 & 0 & 0 & 0 & 0 & 0.3735 & 0.5954 \end{bmatrix}$$

$$w_p(s) = \frac{s + 11.94}{3.981s + 3.777}, \quad w_u(s) = \frac{s + 15.81}{3.162s + 50}$$

$$W_p(s) = w_p(s)I, \quad W_u(s) = w_u(s)I$$

C. FLYBARLESS HELICOPTER

$$x = [\phi, \theta, p, q, a, b, \text{u}, \text{v}]^T \quad \text{[SI units]}$$

$$\bar{x} = [0, 0, 0, 0, 0, 0, 0, 0, 0, 0]^T$$

$$C = \begin{bmatrix} 0 & 0 & 1.382 & 0.986 & 0 & 0 & -1.31 & -1.973 \\ 0 & 0 & -0.049 & -1.604 & 0 & 0 & -1.857 & 1.571 \end{bmatrix}$$

$$w_p(s) = \frac{s + 1}{2s + 0.01}, \quad w_u(s) = \frac{0.7s + 0.111}{0.158s + 0.050}$$

$$W_p(s) = w_p(s)I, \quad W_u(s) = w_u(s)I$$

ACKNOWLEDGMENT

The authors would like to thank Ric Wehling, Johnny Evers, Pat Bradshaw, and Willard Larkin for their longstanding support of this research and for many insightful conversations.

REFERENCES

[1] G. K. Taylor and H. G. Krapp, "Sensory systems and flight stability: What do insects measure and why?" *Adv. Insect Physiol.*, vol. 34, pp. 231–316, 2007, doi: 10.1016/S0065-2806(07)34005-8.

[2] J. Humbert, R. Murray, and M. Dickinson, "Sensorimotor convergence in visual navigation and flight control systems," in *Proc. 16th IFAC World Congr.* Amsterdam, The Netherlands: Elsevier, 2005, pp. 253–258.

[3] E. J. Warrant, "Sensory matched filters," *Current Biol.*, vol. 26, no. 20, pp. 976–980, Oct. 2016.

[4] H. G. Krapp and R. Hengstenberg, "Estimation of self-motion by optic flow processing in single visual interneurons," *Nature*, vol. 384, no. 6608, pp. 463–466, Dec. 1996.

[5] M. O. Franz and H. G. Krapp, "Wide-field, motion-sensitive neurons and matched filters for optic flow fields," *Biol. Cybern.*, vol. 83, no. 3, pp. 185–197, Aug. 2000.

[6] S.-Y. Takemura et al., "A visual motion detection circuit suggested by *Drosophila* connectomics," *Nature*, vol. 500, no. 7461, pp. 175–181, Aug. 2013.

[7] M. S. Maisak, J. Haag, G. Ammer, E. Serbe, M. Meier, A. Leonhardt, T. Schilling, A. Bahl, G. M. Rubin, A. Nern, B. J. Dickson, D. F. Reiff, E. Hopp, and A. Borst, "A directional tuning map of *Drosophila* elementary motion detectors," *Nature*, vol. 500, no. 7461, pp. 212–216, Aug. 2013.

[8] J. K. Lappalainen et al., "Connectome-constrained networks predict neural activity across the fly visual system," *Nature*, vol. 634, no. 8036, pp. 1132–1140, Oct. 2024, doi: 10.1038/s41586-024-07939-3.

[9] J. Pujol-Martí and H. López-Schier, "Developmental and architectural principles of the lateral-line neural map," *Frontiers Neural Circuits*, vol. 7, p. 47, Mar. 2013.

[10] S. Coombs and J. Montgomery, "The role of flow and the lateral line in the multisensory guidance of orienting behaviors," in *Flow Sensing in Air and Water*, J. M. H. Bleckmann and S. Coombs, Eds., Berlin, Germany: Springer, 2014, pp. 65–101.

[11] R. C. Elson, "Integration of wing proprioceptive and descending exteroceptive sensory inputs by thoracic interneurones of the locust," *J. Experim. Biol.*, vol. 128, no. 1, pp. 193–217, Mar. 1987.

[12] B. R. Aiello, K. E. Stanchak, A. I. Weber, T. Deora, S. Sponberg, and B. W. Brunton, "Spatial distribution of campaniform sensilla mechanosensors on wings: Form, function, and phylogeny," *Current Opinion Insect Sci.*, vol. 48, pp. 8–17, Dec. 2021.

[13] J. S. Humbert and A. M. Hyslop, "Bioinspired visuomotor convergence," *IEEE Trans. Robot.*, vol. 26, no. 1, pp. 121–130, Feb. 2010.

[14] A. Hyslop, H. G. Krapp, and J. S. Humbert, "Control theoretic interpretation of directional motion preferences in optic flow processing interneurons," *Biol. Cybern.*, vol. 103, no. 5, pp. 353–364, Nov. 2010.

[15] A. M. Hyslop and J. S. Humbert, "Autonomous navigation in three-dimensional urban environments using wide-field integration of optic flow," *J. Guid., Control, Dyn.*, vol. 33, no. 1, pp. 147–159, Jan. 2010.

[16] P. Xu, J. S. Humbert, and P. Abshire, "Analog VLSI implementation of wide-field integration methods," *J. Intell. Robotic Syst.*, vol. 64, nos. 3–4, pp. 465–487, Dec. 2011.

[17] J. S. Humbert, H. G. Krapp, J. D. Baeder, C. Badrya, I. L. Dawson, J. Huang, A. Hyslop, Y. S. Jung, C. Lutkus, B. Mortimer, I. Nagesh, C. Ruah, S. Walker, Y. Yang, R. W. Żbikowski, and G. K. Taylor, "Motion vision is tuned to maximize sensorimotor energy transfer in blowfly flight," *bioRxiv*, Mar. 2024.

[18] M. van de Wal and B. de Jager, "A review of methods for input/output selection," *Automatica*, vol. 37, no. 4, pp. 487–510, Apr. 2001.

[19] B. Wittenmark and M. E. Salgado, "Hankel-norm based interaction measure for input–output pairing," *IFAC Proc. Volumes*, vol. 35, no. 1, pp. 429–434, 2002.

[20] M. M. Farsangi, Y. H. Song, and K. Y. Lee, "Choice of FACTS device control inputs for damping interarea oscillations," *IEEE Trans. Power Syst.*, vol. 19, no. 2, pp. 1135–1143, May 2004.

[21] C. Westermayer, A. Schirrer, M. Hemedi, and M. Kozek, "An advanced criterion for optimal actuator and sensor placement on complex flexible structures," *IFAC Proc. Volumes*, vol. 42, no. 2, pp. 114–119, 2009.

[22] T. H. Summers, F. L. Cortesi, and J. Lygeros, "On submodularity and controllability in complex dynamical networks," *IEEE Trans. Control Netw. Syst.*, vol. 3, no. 1, pp. 91–101, Mar. 2016.

[23] K. K. Chen and C. W. Rowley, "H_2 optimal actuator and sensor placement in the linearised complex Ginzburg–Landau system," *J. Fluid Mech.*, vol. 681, pp. 241–260, Aug. 2011.

[24] A. Krause, J. Leskovec, C. Guestrin, J. Van Briesen, and C. Faloutsos, "Efficient sensor placement optimization for securing large water distribution networks," *J. Water Resour. Planning Manage.*, vol. 134, no. 6, pp. 516–526, Nov. 2008.

[25] S. Takahashi, Y. Sasaki, T. Nagata, K. Yamada, K. Nakai, Y. Saito, and T. Nonomura, "Sensor selection by greedy method for linear dynamical systems: Comparative study on Fisher-information-matrix, observability-gramian and Kalman-filter-based indices," *IEEE Access*, vol. 11, pp. 67850–67864, 2023.

[26] S. Joshi and S. Boyd, "Sensor selection via convex optimization," *IEEE Trans. Signal Process.*, vol. 57, no. 2, pp. 451–462, Feb. 2009.

[27] A. K. Singh and J. Hahn, "Determining optimal sensor locations for state and parameter estimation for stable nonlinear systems," *Ind. Eng. Chem. Res.*, vol. 44, no. 15, pp. 5645–5659, Jul. 2005.

[28] D. Georges, "The use of observability and controllability gramians or functions for optimal sensor and actuator location in finite-dimensional systems," in *Proc. 34th IEEE Conf. Decis. Control*, vol. 4, Dec. 1995, pp. 3319–3324.

[29] H. R. Shaker and M. Tahavori, "Optimal sensor and actuator location for unstable systems," *J. Vibrat. Control*, vol. 19, no. 12, pp. 1915–1920, Sep. 2013.

[30] A. Hać and L. Liu, "Sensor and actuator location in motion control of flexible structures," *J. Sound Vibrat.*, vol. 167, no. 2, pp. 239–261, Oct. 1993.

[31] K. Yamada, Y. Sasaki, T. Nagata, K. Nakai, D. Tsubakino, and T. Nonomura, "Efficient sensor node selection for observability gramian optimization," *Sensors*, vol. 23, no. 13, p. 5961, Jun. 2023.

[32] M. S. Sakha and H. R. Shaker, "Optimal sensors and actuators placement for large-scale unstable systems via restricted genetic algorithm," *Eng. Comput.*, vol. 34, no. 8, pp. 2582–2597, Nov. 2017.

[33] K. Zhou, G. Salomon, and E. Wu, "Balanced realization and model reduction for unstable systems," *Int. J. Robust Nonlinear Control*, vol. 9, no. 3, pp. 183–198, Mar. 1999.

[34] A. J. Krener and K. Ide, "Measures of unobservability," in *Proc. 48th IEEE Conf. Decis. Control (CDC) Held Jointly 28th Chin. Control Conf.*, Dec. 2009, pp. 6401–6406.

[35] B. T. Hinson and K. A. Morgansen, "Observability-based optimal sensor placement for flapping airfoil wake estimation," *J. Guid., Control, Dyn.*, vol. 37, no. 5, pp. 1477–1486, Sep. 2014.
[36] B. Boyacioğlu, M. Babaei, A. H. Mamo, S. Bergbreiter, T. L. Daniel, and K. A. Morgansen, "Sensor placement for flapping wing model using stochastic observability gramians," 2023, *arXiv:2310.00127*.
[37] P. C. Müller and H. I. Weber, "Analysis and optimization of certain qualities of controllability and observability for linear dynamical systems," *Automatica*, vol. 8, no. 3, pp. 237–246, May 1972.
[38] A. M. A. Hamdan and A. M. Elabdalla, "Geometric measures of modal controllability and observability of power system models," *Electric Power Syst. Res.*, vol. 15, no. 2, pp. 147–155, Oct. 1988.
[39] B. Herrmann, P. J. Baddoo, S. T. M. Dawson, R. Semaan, S. L. Brunton, and B. J. McKeon, "From resolvent to gramians: Extracting forcing and response modes for control," 2023, *arXiv:2301.13093*.
[40] B. Marx, D. Koenig, and D. Georges, "Optimal sensor and actuator location for descriptor systems using generalized gramians and balanced realizations," in *Proc. Amer. Control Conf.*, vol. 3, 2004, pp. 2729–2734.
[41] H. R. Shaker and J. Stoustrup, "An interaction measure for control configuration selection for multivariable bilinear systems," *Nonlinear Dyn.*, vol. 72, nos. 1–2, pp. 165–174, Apr. 2013.
[42] K. Manohar, J. N. Kutz, and S. L. Brunton, "Optimal sensor and actuator selection using balanced model reduction," *IEEE Trans. Autom. Control*, vol. 67, no. 4, pp. 2108–2115, Apr. 2022.
[43] K. B. Lim and W. Gawronski, "Hankel singular values of flexible structures in discrete time," *J. Guid., Control, Dyn.*, vol. 19, no. 6, pp. 1370–1377, Nov. 1996.
[44] K. B. Lim, "Disturbance rejection approach to actuator and sensor placement," *J. Guid., Control, Dyn.*, vol. 20, no. 1, pp. 202–204, Jan. 1997.
[45] G. C. Smith and R. L. Clark, "Frequency-shaping with spatial compensators," *J. Intell. Mater. Syst. Struct.*, vol. 11, no. 10, pp. 811–820, Oct. 2000.
[46] Y. Cao and P. Saha, "Control structure selection for unstable processes using Hankel singular value," in *Computer Aided Chemical Engineering*, vol. 14. Amsterdam, The Netherlands: Elsevier, 2003, pp. 383–388.
[47] W. K. Gawronski, *Advanced Structural Dynamics and Active Control of Structures* (Mechanical Engineering Series), 1st ed., New York, NY, USA: Springer, 2004.
[48] P. Ambrosio, F. Resta, and F. Ripamonti, "An H_2 norm approach for the actuator and sensor placement in vibration control of a smart structure," *Smart Mater. Struct.*, vol. 21, no. 12, Nov. 2012, Art. no. 125016.
[49] M. C. De Oliveira and J. C. Geromei, "Linear output feedback controller design with joint selection of sensors and actuators," *IEEE Trans. Autom. Control*, vol. 45, no. 12, pp. 2412–2419, Dec. 2000.
[50] K. Morris, M. A. Demetriou, and S. D. Yang, "Using H_2-control performance metrics for the optimal actuator location of distributed parameter systems," *IEEE Trans. Autom. Control*, vol. 60, no. 2, pp. 450–462, Feb. 2015.
[51] G. J. Balas and P. M. Young, "Sensor selection via closed-loop control objectives," *IEEE Trans. Control Syst. Technol.*, vol. 7, no. 6, pp. 692–705, Nov. 1999.
[52] W. Liu, Z. Hou, and M. A. Demetriou, "A computational scheme for the optimal sensor/actuator placement of flexible structures using spatial H_2 measures," *Mech. Syst. Signal Process.*, vol. 20, no. 4, pp. 881–895, May 2006.
[53] A. Argha, S. W. Su, and A. Savkin, "Optimal actuator/sensor selection through dynamic output feedback," in *Proc. IEEE 55th Conf. Decis. Control (CDC)*, Dec. 2016, pp. 3624–3629.
[54] J. A. Taylor, N. Luangsomboon, and D. Fooladivanda, "Allocating sensors and actuators via optimal estimation and control," *IEEE Trans. Control Syst. Technol.*, vol. 25, no. 3, pp. 1060–1067, May 2017.
[55] L. Huang, J. Wu, Y. Mo, and L. Shi, "Joint sensor and actuator placement for infinite-horizon LQG control," *IEEE Trans. Autom. Control*, vol. 67, no. 1, pp. 398–405, Jan. 2022.
[56] D. Kasinathan and K. Morris, "H_∞-optimal actuator location," *IEEE Trans. Autom. Control*, vol. 58, no. 10, pp. 2522–2535, Oct. 2013.
[57] T. Singh, M. De Mauri, W. Decré, J. Swevers, and G. Pipeleers, "Feedback control of linear systems with optimal sensor and actuator selection," *J. Vibrat. Control*, vol. 27, nos. 11–12, pp. 1250–1264, Jun. 2021.
[58] U. Munz, M. Pfister, and P. Wolfrum, "Sensor and actuator placement for linear systems based on H_2 and H_∞ optimization," *IEEE Trans. Autom. Control*, vol. 59, no. 11, pp. 2984–2989, Nov. 2014.
[59] S. Nugroho, A. F. Taha, T. Summers, and N. Gatsis, "Simultaneous sensor and actuator selection/placement through output feedback control," in *Proc. Annu. Amer. Control Conf. (ACC)*, Jun. 2018, pp. 4159–4164.
[60] B. Jin, S. J. Illingworth, and R. D. Sandberg, "Optimal sensor and actuator placement for feedback control of vortex shedding," *J. Fluid Mech.*, vol. 932, p. 2, Feb. 2022.
[61] S. Boyd, L. El Ghaoui, E. Feron, and V. Balakrishnan, *Linear Matrix Inequalities in System and Control Theory* (SIAM Studies in Applied Mathematics), vol. 15. Philadelphia, PA, USA: Society for Industrial and Applied Mathematics, 1994.
[62] K. Glover, "Robust stabilization of linear multivariable systems: Relations to approximation," *Int. J. Control*, vol. 43, no. 3, pp. 741–766, Mar. 1986.
[63] B. A. Francis, *A Course in H_∞ Control Theory* (Lecture Notes in Control and Information Sciences), vol. 88. Berlin, Germany: Springer, 1987.
[64] G. E. Dullerud and F. G. Paganini, *A Course in Robust Control Theory: A Convex Approach*. New York, NY, USA: Springer-Verlag, 2000.
[65] R. F. Stengel, *Optimal Control and Estimation*. New York, NY, USA: Dover, 1994.
[66] B. Moore, "Principal component analysis in linear systems: Controllability, observability, and model reduction," *IEEE Trans. Autom. Control*, vol. AC-26, no. 1, pp. 17–32, Feb. 1981.
[67] K. Hausen, "Decoding of retinal image flow in insects," *Rev. Oculomotor Res.*, vol. 5, pp. 203–235, Jan. 1993.
[68] H. G. Krapp, B. Hengstenberg, and R. Hengstenberg, "Dendritic structure and receptive-field organization of optic flow processing interneurons in the fly," *J. Neurophysiol.*, vol. 79, no. 4, pp. 1902–1917, Apr. 1998.
[69] S. Yang, W. Birk, and Y. Cao, "A new controllability index based on Hankel singular value," *IFAC-PapersOnLine*, vol. 53, no. 2, pp. 4662–4667, 2020.
[70] A. Ben-Israel, "Projectors on intersections of subspaces," in *Contemporary Mathematics*, vol. 636. Haifa, Israel: American Mathematical Society, 2015, pp. 41–50.
[71] S. Skogestad and I. Postlethwaite, *Multivariable Feedback Control: Analysis and Design*. Hoboken, NJ, USA: Wiley, 2005.
[72] R. J. Caverly and J. R. Forbes, "LMI properties and applications in systems, stability, and control theory," 2024, *arXiv:1903.0859*.
[73] J. Lofberg, "YALMIP: A toolbox for modeling and optimization in MATLAB," in *Proc. IEEE Int. Conf. Robot. Autom.*, Taipei, Taiwan, Sep. 2004, pp. 284–289.
[74] R. C. Gardner and J. S. Humbert, "Comparative framework for maneuverability and gust tolerance of microhelicopters," *J. Aircr.*, vol. 51, no. 5, pp. 1546–1553, Sep. 2014.
[75] T. L. Mohren, T. L. Daniel, S. L. Brunton, and B. W. Brunton, "Neural-inspired sensors enable sparse, efficient classification of spatiotemporal data," *Proc. Nat. Acad. Sci. USA*, vol. 115, no. 42, pp. 10564–10569, Oct. 2018.
[76] W.-H. Chen, J. Yang, L. Guo, and S. Li, "Disturbance-observer-based control and related methods—An overview," *IEEE Trans. Ind. Electron.*, vol. 63, no. 2, pp. 1083–1095, Feb. 2016.
[77] M. Shen, H. Zhang, S. K. Nguang, and C. K. Ahn, "H_∞ output anti-disturbance control of stochastic Markov jump systems with multiple disturbances," *IEEE Trans. Syst., Man, Cybern., Syst.*, vol. 51, no. 12, pp. 7633–7643, Dec. 2021.

ZOE TURIN received the B.Sc. degree in mechanical engineering from Georgia Institute of Technology, in 2019, and the M.Sc. degree in mechanical engineering from the University of Colorado Boulder, in 2022, where she is currently pursuing the Ph.D. degree in mechanical engineering. Her research focuses on the translation of distributed sensing principles from biology to engineering applications.

GRAHAM K. TAYLOR received the M.A. degree in biological sciences from the Pembroke College, in 1998, and the D.Phil. degree in zoology from the Jesus College, Oxford, U.K., in 2003. He has held several junior and advanced research positions, including the prestigious Royal Society University Research Fellowship and RCUK Academic Fellowship with the Department of Zoology, University of Oxford, where he is currently a Professor of mathematical biology with the Department of Biology; and the Deputy Head of the Mathematical, Physical and Life Sciences (MPLS) Division. As a Leader of the Oxford Flight Group, his research is at the crossover of biology with engineering and focuses on problems in guidance, navigation, and control, with projects spanning birds, bats, insects, and autonomous systems.

HOLGER G. KRAPP received the Diploma degree in biology from the University of Tübingen, Germany, in 1992, and the Dr. rer. nat. (Ph.D.) degree in neural basis of optic flow processing from the Max-Planck Institute (MPI) for Biological Cybernetics, Tübingen, in 1995. After postdoctoral positions with MPI, Caltech, and Bielefeld University, he was a temporary Lecturer in sensory neuroscience with the Department of Zoology, University of Cambridge, U.K., until 2005. He is currently a Professor of systems neuroscience with the Department of Bioengineering, Imperial College London, where he studies neural mechanisms underlying biological design principles of sensorimotor control with application potential for autonomous robotic systems.

EMILY JENSEN (Member, IEEE) received the B.Sc. degree in engineering, mathematics and statistics from UC Berkeley, in 2015, and the Ph.D. degree in electrical and computer engineering from the University of California at Santa Barbara, in 2020. She is an Assistant Professor with the Department of Electrical, Computer and Energy Engineering, University of Colorado Boulder. She has held positions as a Postdoctoral Researcher with the University of California at Berkeley and Northeastern University. She has received the UC Regents' Graduate Fellowship, in 2016, and the Zonta Amelia Earhart Graduate Fellowship, in 2019.

J. SEAN HUMBERT (Member, IEEE) received the B.Sc. degree in mechanical engineering from the University of California Davis, in 1997, and the M.Sc. and Ph.D. degrees in mechanical engineering from California Institute of Technology, in 1999 and 2005, respectively. From 2005 to 2014, he was an Assistant Professor and an Associate Professor of aerospace engineering with the University of Maryland, College Park. He is currently a Professor of mechanical engineering and the Director of the Robotics Program, University of Colorado Boulder. His research interests include robotics, flight dynamics, and control coupled with perception and reduction principles in biology.